CLM -R147 FINAL DRAFT

POTASSIUM AND SODIUM COOLING FOR FUSION REACTOR BLANKETS.

R.G. OWEN AND L.J. BAKER.

(1977)

2nd draft

CLM-R147

Potassium and sodium Cooling for Fusion Reactor Blankets.

R.G. Owen* and L.J. Baker+

* Thermodynamics Division

+ Materials Physics Division

A.E.R.E.

Harwell, Oxon.

Culham Laboratory,

Abingdon,

Oxfordshire.

Potassium and Sodium Cooling for Fusion Reactor Blankets

R. G. OWEN* AND L. J. BAKER+

* Thermodynamics Division

\+ Materials Physics Division
A.E.R.E.
Harwell, Oxon.

ABSTRACT

A potassium cooled fusion reactor blanket is analysed for maximum wall loading. Two conceptual designs are postulated, one utilising a once-through evaporation process - the other employing wicked boiling surfaces. The wicked configuration is found to ~~be preferable,~~ give a high wall loading thermal constraints and limitations on stress in the structure, limiting the maximum wall loading to approximately 5 MW/m^2. This is an ~~improvement on~~ increase over the maximum wall loading of a simple direct lithium cooled fusion reactor blanket and is comparable to that achievable in a helium cooled blanket.

The potassium cooled fusion blanket is compared with other systems and its advantages and disadvantages are discussed.

CONTENTS

Appendices:-

LIST OF FIGURES

1. INTRODUCTION

Research into the physics of fusion has progressed to the stage where studies may now be undertaken on the design and optimisation of fusion reactor structures and systems.

The three principal fusion reactor systems provide for:

(a) Plasma Confinement:

The reacting plasma must be isolated from materials in the surrounding blanket. High magnetic fields are the principal means of confinement and several different field configurations have been proposed. This study assumes a Tokamak confinement scheme in which the magnetic field transform necessary for plasma stability and equilibrium is provided by diffusion-driven currents. The confining magnetic fields are toroidal in shape and are provided by super-conducting magnets equispaced around the torus. For a reactor output of 2500 MW(e), major and minor diameters of the toroidal plasma ~~would be approximately~~ can be a large as 20m and 3m respectively - the ~~exact~~ dimensions depending on the wall loading capability of the cooling blanket which surrounds the plasma. (Figure 1 gives a general view of a steady state Tokamak fusion reactor). Protection must be given to the copper or aluminium stabilizing component of the magnet conductor and to the super-conductors to prevent damage by neutrons and consequent loss of conductivity. Structure and shielding material must, therefore, be provided to limit this radiation damage.

(b) Breeding:

The first generation of fusion reactors will be based on the deuterium-tritium fuel cycle because it has the highest reaction rate at low plasma temperatures. Tritium, however, only occurs in nature in very small quantities so that ~~artificial~~ breeding is necessary to maintain a fuel supply. This is achieved by surrounding the plasma with a nuclear blanket containing ~~natural~~ lithium, using (n,α) reactions in both ^{6}Li and ^{7}Li to breed tritium.

(c) Thermalisation of Neutron Energy

Conversion of Neutron and Bremsstrahlung energy produced by the D-T reaction into heat requires the plasma to be surrounded by a blanket of suitable absorbing material. In addition to breeding tritium, lithium has the advantage of being a good moderator, due to its low atomic mass. Heat released in the lithium by thermalisation of the 14 MeV D-T neutrons is the primary source of energy for external power generation. As liquid lithium is an excellent heat transfer fluid, its circulation through the cooling blanket would seem to be an ideal means for efficient removal of this energy. However, the lithium, being a conducting liquid metal, suffers large magnetohydrodynamic pressure losses when it flows transversely to the confining magnetic fields.

In addition, the flow rate must ~~be sufficiently high to~~ provide the necessary heat transfer rate, of the coolant, without excessive temperature rise. Restrictions on stresses within the blanket structure and on coolant pumping power have been shown for a particular reactor model limit the maximum wall loading to about 3-4 MW/m^2 [1,2]. The possibility of using lithium in a boiling mode as the blanket coolant is obviated by the high temperature of lithium in the two phase region (e.g. 1340°C at 1 bar). Lifespan and structure fraction requirements on the cooling blanket cannot be attained at such operating temperatures with the structural materials currently available.

It has been suggested [3] that indirect cooling of the lithium blanket by helium gas at high pressure would improve the maximum wall loading, because helium is not subject to magnetohydrodynamic losses. Moreover, the design of a helium-cooled blanket is independent of the magnetic configuration required for plasma confinement.

Calculations[3] have shown that a helium cooled blanket is thicker than a corresponding directly cooled blanket and that compressor power requirements are as much as 2% of the reactor output. An improved wall loading of 6 MW/m^2 is attainable with a helium cooled blanket for a similar reactor model though such a blanket would be a complicated and hence, expensive item.

An alternative means of indirect cooling utilises potassium metal as the heat transfer fluid. Liquid potassium is pumped into the cooling blanket in which it is evaporated and from which it emerges as a saturated vapour. This system, like the direct lithium cooling system, incurs a magnetohydrodynamic pressure loss wherever liquid potassium traverses the confining magnetic field. However, the potassium cooled blanket has several advantages. The large heat transfer coefficient associated with boiling permit small coolant volume within the blanket. The large enthalpy change of potassium with phase change allows lower flow rates than for a direct lithium cooled blanket. Near the front wall of the cooling blanket where there is intensive radiation flux, the pressure within the breeding blanket and within the potassium ducts may be maintained at low levels (several bars). As compare with higher pressure coolants, this could permit a better compromise between structur stress and volume fraction in the blanket.

In this report, a study is made of the effectiveness of potassium as a heat transfer fluid for a fusion reactor cooling blanket. Attention is specifically directed to the thermodynamic and neutronic performance of potassium as a coolant and consideration has not been given to the performance of structural materials subject to fast neutron irradiation. This work complements the parallel analysis of a direct lithium cooled blanket by Hunt and Hancox[1,2] and the study of an indirect helium cooled blanket by Mitchell and Booth[3]. Although attention in this report is mainly directed at examining potassium as a blanket coolant brief consideration is also given to sodium.

2. THE FUSION REACTOR MODEL

The fusion reactor model used for this study is described in reference 4.* It is a steady-state Tokamak with a reactor electrical output of 2500 MW(e). The

* Since the inception of this study the Culham conceptual reactor model has changed somewhat. The more recent design parameters are compared with the original parameters in appendix L and the effect of these changes on the computed maximum reactor wall loading is not found to be significant.

INSERT P3

The cell is constructed in the following manner. At either end of the cell is a manifold, one being the inlet manifold fed with liquid ~~post~~ potassium, the other the exhaust manifold from which potassium vapour is passed to steam generators external to the reactor. Connecting the two manifolds are straight tubes in which the potassium is vaporized.

toroidal confining magnetic field is provided by 32 superconducting magnets of approximately 8m internal diameter and $1m^2$ cross-section. Figure 2 illustrates one of the segments of the toroidal assembly. The plasma is surrounded by a cellular blanket, itself thermally insulated from, but supported by, a load carrying structure which also forms the magnet shield. Between the cells and the support structure, there are manifolds for circulating the coolant and the lithium (for tritium recovery), these manifolds being connected to penetrations through the shield. Surrounding the magnet shield but structurally separated from it is a cryostat containing the superconducting magnet coils which provide the toroidal magnetic field.

The blanket is cellular in construction[5,6]. The cells containing the lithium are of rectangular cross-section and tapered so that they are close-nested around the plasma, minimising the loss of neutron flux to the magnet shield. They are typically 0.3m wide and 1m long to give the blanket thickness determined by tritium breeding calculations (see figure 3). The front $\frac{3}{4}$ of the cell contains the lithium and cooling ducts while the rear section is the graphite neutron reflector through which the pipes carrying the potassium pass to external manifolds. These manifolds are situated between the cell base and the magnet shield. Small diameter pipes are arranged, similarly, for the circulation of lithium. Th total duct area for circulation of both lithium and coolant is not greater than 0.1 of the external surface area of the magnet shield.

3. DESCRIPTION OF THE POTASSIUM COOLED CELL:

Magnetohydrodynamic pressure loss occurs in coolant ducts whenever single phase liquid potassium or two phase liquid/vapour potassium flows transverse to the magnetic field within the superconducting winding. For magnetic field strengths characteristic of fusion reactors, this MHD pressure drop ~~is~~ carbe several orders of magnitude greater than the frictional pressure drop. In order to minimise coolant pumping power and structure volume within the blanket cells it is necessary to limit liquid phase and two phase coolant flow paths transverse to the magnetic field. This may be accomplished either by confining the boiling coolant to channels aligned with the magnetic field or by utilising overlayed with porous layers. ~~surfaces.~~ The first of these arrangements is termed the once-through evaporator configuration, the second, the wicked configuration.

A schematic diagram of a potassium once-through evaporating configuration is shown in figure 3. A Liquid potassium is pumped through access ducts in the magnet winding and shield and enters the cell as subcooled liquid. The sub-cooled liquid flows towards the front wall of the cell and is divided between coolant tubes which pass through the bulk lithium and those which cool the cell wall. Sufficient subcooling is allowed to ensure that flow is single phase liquid to the front wall.

INSERT

INSERT 1 (P4)

The characteristic temperature in the coolant boiling channels is dependent on the pressure levels in these channels, increase in pressure increasing the ~~corresponding~~ temperature. For potassium at 1 atmosphere pressure (absolute) the temperature is 760°C, the corresponding figure for sodium is 883°C.

INSERT 2 (p4)

The cell has manifolds at each end, the liquid potassium entering the cell through the inlet manifold and the potassium vapour exhausting through the outlet manifold. The manifolds are connected by tubes or more simply by rectangular channels ~~which~~ the spaces between and which are filled with lithium. The internal surfaces of each of the rectangular coolant channels are overlayed with a ~~pour~~ porous material (referred to as a wick). The liquid potassium is pumped into the porous wick which has a large number of channels (arteries) within the porous layer to give even distribution of liquid potassium to the heated channel surfaces. The coolant channels are roughly aligned with the toroidal magnetic field within the windings. The potassium is ~~boiled~~ evaporated within the porous ~~wick~~ surfaces and ~~flows~~ the vapour flows to the core of each coolant channel.

The two-phase boiling region is aligned parallel to the magnetic field within the magnet windings. Helical inserts are provided to ensure high coolant mass quality within the field aligned region. The tube spacing is close near the front wall of the cell and increases towards the rear of the cell to even out heat input and materials utilisation throughout the cell.

A diagram of the wicked configuration is provided in figure 4. ~~The boiling surfaces are overlayed with a porous sinter into which liquid potassium is pumped and from which it is boiled.~~ The number of overlayed surfaces is such that the total surface area is sufficient to boil off the required coolant flow. The boiling surfaces are spaced to even out the heat input and materials utilisation along the length of the cell. ~~The overlayed plates are aligned with the magnetic field and arteries are provided for even distribution of potassium.~~ Wick parameters (voidage fraction etc) are optimised to give maximum liquid flow to the solid surfaces while maintaining low entrainment of liquid in the vapour stream.

A comparison of the two configurations may be obtained from calculations of respective primary circuit pressure losses and maximum wall loadings for a fusion reactor of output 2500 MW(e). The maximum wall loading is defined as the maximum energy flux through the front wall of the blanket within the limitations of structure stress, structure volume, breeding gain, coolant pumping power and blanket lifespan.

The main reactor parameters (assuming a constant torus aspect ratio) are given in table 1 for wall loadings of 1, 5 and 10 MW/m^2. Technical calculations for the wicked and once-through evaporating configurations, based on these figures, are presented in sections 4 and 5 respectively.

4. WICKED CONFIGURATION - A PERFORMANCE ANALYSIS:

The primary coolant circuit for the wicked configuration is given in Appendix B. The component pressure drops for the circuit are comprised of two types; magnetohydrodynamic pressure losses and frictional pressure losses. Magnetohydrodynamic pressure losses occur both in the cell inlet manifold and in the wicked boiling region. In the cell inlet header, the liquid potassium primarily flows transversely to the magnetic field within the superconducting winding whereas, in the wick, flow of liquid potassium is predominantly aligned with the magnetic field lines and has only a small transverse velocity component. Frictional pressure losses occur in all portions of the primary circuit. In particular the frictional pressure drop in the following items must be calculated - the supply line from the pump to the reactor, the inlet and outlet ducts to each cell, the wicks, the external heat exchangers and associated ducting.

In Appendix B these various pressure losses are computed for reactor first wall loadings of 1, 5 and 10 MW/m^2. It is observed that the magnetohydrodynamic pressure losses dominate the frictional pressure losses and that the frictional pressure losses in the vapour-carrying ducts are only appreciable as the vapour velocity nears its ~~critical value~~ sonic limit. In order to minimise the primary circuit pressure drop the coolant supply and outlet ducts to each coolant cell must be made as large as possible consistent with neutron economy and space limitations.

The total area for ducting is fixed by assuming that the maximum area allowable is 0.1 of the external surface area of the magnet shield. This area is divided between inlet ducting and exhaust ducting of coolant so that overall primary circuit pressure drop is minimised. A limitation on the exit velocity of the potassium vapour is set, however, at a Mach number of 0.3 to ensure that the boiling region is maintained at low pressure. Pressure drop computations of Appendix B show that the MHD pressure drops in the inlet manifold and inlet ducts dominate the primary circuit pressure distribution. The inlet ducts are, therefore, made considerably larger than the exit ducts, in order to minimize coolant pumping power requirements. This does, however, increase the volume of liquid potassium within the cell ~~reducing~~ the cell tritium breeding gain. Breeding calculations for a potassium cooled cell are given in section 8 and have indicated that breeding gain is sufficient for cells of overall length 1 metre.

An analysis of the pressure drop and maximum heat transfer rates in the porous wicks is given in Appendix C. A model is presented of convective boiling in a surface overlayed with a porous sinter when magnetohydrodynamic forces act on the liquid flow in the capillaries. The maximum heat transfer rates, the wick pressure drops and the optimised wick parameters are presented in figure 5, for magnetic field intensities ranging from 1 to 20 tesla. The pressure drop across the wick is found to be small ($\approx 10^3$ N/m^2) and heat transfer rates of the order 1 MW/m^2 are possible for wicks of 1 mm to 1 cm thickness. Considerations of entrainment of liquid potassium from the wick indicate that a wick of minimum thickness 0.5 cm is required. For a notional blanket cell of dimensions (0.3 metre x 1.0 metre x 1.0 metre) the number of required sinter overlayed surfaces may be calculated as a function of front wall loading. It is found that, in principle, at low wall loadings of 1 MW/m^2, only a single wicked plate is required though, in practice, several plates (operating at a reduced heat flux rating) would be used to limit temperature within the lithium. A reasonable number of plates (5-10) is needed at wall loadings of 5-7 MW/m^2 and an excessively large number (20) at a wall loading of 10 MW/m^2. Pumping power requirements are calculated for various wall loadings and are given in Appendix H. It may be seen that pumping power only becomes excessive (greater than 2% of the reactor output) as the front wall loading tends to 10 MW/m^2. Structure fraction within the blanket cell is also given in Appendix H. Typical structure fractions of 6% are attained at wall loading of 7-8 MW/m^2.

The limiting factor in the design of the potassium cooled cell is that imposed by the stressing and creep of the coolant ducts. Although the pressure in the coolant ducts is low in zones of high radiation damage, the coolant ducts operate at temperature levels between 500°C and 900°C and this reduces the yield stress of the structural material. The boiling potassium system has a temperature in the evaporatin region which is constant and independent of load variations. Radiation damage, however, is dependent on wall loading so that design considerations for the cooling ducts of a potassium cooled cell will be similar to those for a lithium cooled cell.(6)

In figure 6 a graph is given in which the maximum front wall loading may be obtained for stress limits of 25, 50 and 100 MN/m^2 in the duct walls. The coolant ducts with greatest stressing, the inlet manifolds, operate at a temperature of approximately 550°C and at this temperature a maximum permissible stress of 50 MN/m^2 would appear to be appropriate. From figure 6, this limits the maximum front wall loading to approximately 5.5 MW/m^2. This rating is 1.5 MW/m^2 higher than that possible with a direct lithium cooled blanket.(4) The increase derives primarily from the lower potassiu flowrates necessary to achieve a specific heat removal rate from a blanket cell. The maximum stressing of the cooling ducts is directly dependent on the magnetohydrodynami pressure drop in the primary coolant circuit. The latter is roughly proportional to the coolant flowrate and to the square of the maximum magnetic field intensity. The square of the maximum magnetic field intensity also increases rapidly with wall loadin such that at high wall loadings ($\gtrsim 5$ MW/m^2), stressing of the blanket structure increases rapidly with first wall loading. This effectively sets a cut-off on permissible wall loadings and is an inherent feature of the use of a liquid metal as a fusion blanket coolant.

5. THE ONCE-THROUGH EVAPORATOR CONFIGURATION - A PERFORMANCE ANALYSIS

The once-through evaporator configuration differs from the wicked configuration only in the arrangement of the boiling region. In the once-through evaporator, boiling takes place in circular ducts aligned with the magnetic field. The coolant flow is divided between tubes which cool the cell wall and those which cool the bulk lithium and the spacing of these ducts is arranged to even out the heat input.

An analysis of the pressure drop and critical heat flux for such boiling channels is given in Appendix G. Because the flow is aligned with the magnetic field, the turbulence in the liquid phase is damped and for straight tubes the pressure drop in two phase flow can be estimated from Hunt and Hancox (1). The critical heat flux for the boiling of saturated potassium in 2 cm diameter tubes may be calculated to be approximately 3 MW/m^2 (Appendix G) in a non-magnetohydrodynamic

situation. The effect of an axial magnetic field is to slow the movement of bubbles away from the wall because there is resistance to the motion of the liquid transverse to the magnetic field. This effect, coupled with the lower level of mixing in the liquid phase may cause dryout of the liquid film at the duct wall at low mass qualities. The cell is a heat flux controlled unit and any large reduction in overall heat transfer coefficient may lead to excessively high duct wall temperatures. Twisted tapes are commonly used to prevent dryout at low qualities. These act to force the liquid onto the heated walls and are common practice in liquid metal boilers.

In a magnetohydrodynamic situation, however, the swirl component of the two phase flow has to traverse the dominant magnetic field and incurs a pressure drop several orders of magnitude greater than the purely frictional pressure drop. An estimate of this MHD pressure drop is given in Appendix G. It may be observed that this pressure drop is considerable and raises the pressure in the cooling tubes in the vicinity of the front wall of the blanket where radiation damage is highest.

A further problem arises with the once-through evaporator arrangement. Ideally the heat transfer characteristics of the cell should be arranged so that dryout occurs at the junction of the cooling ducts and the outlet manifold. This would avoid having a two phase flow (with its large MHD pressure loss) in the outlet manifold where the flow is transverse to the magnetic field. However, there is a danger that a reactor transient could then cause the dryout point to move along the cooling ducts towards the inlet manifold and eventually cause the coolant channels to dry-out completely. In order to prevent such a possibility, some two phase pressure drop in the outlet manifold would have to be accepted. Calculation of pressure drop in the outlet manifold may be estimated from Owen, Hunt and Collier.(7)

The once-through evaporator thus incurs a higher pressure drop than does the over-layed arrangment (appendices C and G). Because stressing of the blanket structure is a primary limitation on reactor performance, in this respect, the once-through evaporator is inferior to the wicked configuration.

6. STRUCTURE AND LITHIUM TEMPERATURES FOR BOTH CELL CONFIGURATIONS:

Within the blanket region, structure and lithium temperatures are governed by the heat deposition profile. Bremsstrahlung and synchroton radiation are absorbed within the front wall and may be considered as a constant heat flux at the front wall of the blanket. The heat deposition profiles for wall loadings of 1, 5 and 10 MW/m^2 are based on the data of Blow(9) and scaled on a pro-rata basis. The 10 MW/m^2 profile is shown in figure 9. This heat deposition data is adequate for the present study and has been adjusted for the increase in blanket thickness which compensates for coolant voidage within the cell. The data of

Blow[9] assumes a 6% structure fraction, which is a reasonable figure for a potassium cooled cell. The radiation flux at the plasma confining wall is assumed to be five per cent of the neutron power loading and small variations about this value have little influence on blanket cooling design.

Within the lithium, Parkin et al[10] have shown that the magnetic field prevents the formation of convection currents and that heat transfer through the lithium may be considered as a pure conduction problem. The conservative assumption is made in calculating structure temperatures, that all heat deposition occurs within the lithium or structure, not in the coolant. The following additional assumptions are made in calculating structure and lithium temperatures within the cell:

1) The potassium temperature is the saturation temperature at approximately two atmospheres pressure.
2) The temperature rises for volumetric and surface heating have been calculated assuming constant thermal conductivity for the structure.
3) The structural material is assumed to be TZM.
4) Spacing of the cooling ducts/plates is designed to even out heat input.
5) For calculating structure temperatures between cooling channels, thermal shunting due to the lithium is neglected. The temperature rise is proportional to q/k. Now $q_{TZM} \approx 3/2\, q_{Li}$ and $k_{TZM} \approx k_{Li}$, so that this assumption ~~will~~ could be conservative by overestimating structure temperatures.
6) The temperature of the cooling ducts is the sum of the potassium temperature and the tube wall temperature rise at the specific location. The heat flux for a given cooling duct/plate is considered constant, hence the latter temperature rise is constant along a cooling channel.
7) The cell body and lithium maximum temperatures include the volumetric and radiation heating between the cooling tube and the test location.

The structure and lithium temperatures are calculated at several locations within the cell and the results are summarised in table 3 for a front wall loading of 7.5 MW/m^2. The temperatures given are the maxima for the material at the given location e.g. the tube temperature is that of the outer tube surface. Duct temperatures are given together with cell wall temperatures.

From table 3 it may be observed that the maximum structure temperature is approximately 900°C and the maximum lithium temperature about 1100°C. The latter is sufficiently below the boiling point of lithium at low pressures (several bars) to ensure that pressurisation of the blanket does not occur. The former temperature is such that compatibility of structural materials with potassium and lithium can be achieved within the timescale of reactor development. As discussed in the following section, much progress towards this end has already been achieved by NASA research for the space programme.

7. MATERIALS SELECTION AND COMPATIBILITY:

The utilisation of potassium as a coolant and lithium as a breeding material necessitates the choice of a structural material which is compatible with both these liquid materials. Corrosion by alkali metals may be reduced to negligible amounts at temperatures up to 1100°C by the use of structural materials that include as constituents, the oxygen gettering elements Hf and Zr and by minimising the oxygen content everywhere in the system. Specifications have been formulated for the maximum tolerable oxygen contents of the liquid metal and the containment.[11, 12]

A test loop of Nb-1Zr showed negligible attack after 5000 hr. of exposure to flowing two-phase potassium at temperatures close to 1100°C[12]. The tantalum alloy T-111 has withstood 10,000 hrs with potassium boiling on one surface and pumped lithium at 1230°C flowing over the other surface.[13]

Creep resistant alloys capable of operating for three or more years in an alkali metal system have been developed. This has been accomplished by solid-solution strengthening of refractory metals with other high melting point metals, by dispersion strengthening with interstitial elements such as carbon and nitrogen and by proper fabrication and heat treatment[11,14]. Figure 10 presents curves of 10,000 hr. creep strengths vs. temperature for several alloys. The second stage creep rate is essentially constant during long exposures to constant conditions of stress and temperature[15].

The Molybdenum alloys TZM, and TZC, have been shown to be resistant to erosion in alkali metal systems and are also compatible with lithium. NASA research for the space programme has initiated research into reactor powered Rankine cycles and a life of 20,000 hrs (2.28 years) is postulated as reasonable for tantalum T-111 alloy operating between liquid lithium and boiling potassium at a temperature of approximately 1150°C. 20,000 hours is, however, a short timespan when considering reactor applications. There is a dearth of test data for the timescales (20,000 - 100,000 hours) which would be required for the present application.

The University of Wisconsin Fusion Reactor Study[16] has detailed four possible candidates for the structural material of a fusion blanket. These are 316 stainless steel, Nb-1Zr, V-20 Ti and TZM, and of these Nb-1Zr and TZM are compatible with potassium to temperatures of at least 1100°C. A comparison of the relative merits

of TZM and Nb-1Zr is given in Table 2. The University of Wisconsin reactor group correctly points out that a qualified metal industry is not currently available for either TZM or Nb-1Zr and that implementation of rigid quality assurance programs for production of these alloys is a major effort. The austenitic stainless steels (which have a reasonably qualified industry behind them) are only suitable for use with lithium to 500°C and with potassium up to a temperature of 850°C, both of which are too low for the present requirements.

V-20Ti is a specialized alloy which suffers corrosion in reactor grade alkali metals and is hence not suitable for use in a potassium cooled blanket.

The properties of the alloys during irradiation are also of great importance. The most severe of these problems is irradiation induced embrittlement for which there is a lack of data both for Nb-1Zr and for TZM. The TZM alloy is, however, less susceptible to interstitial embrittlement than is the niobium alloy. TZM is favoured over Nb-1ZR because of its lower tritium permeation but the latter alloy permits lower fabrication costs for high quality blanket components than does TZM.

In summary, the choice of a potassium blanket structural material is not a simple one, and no single alloy possesses all the necessary qualities. Nevertheless, TZM probably represents the best choice at the present time though more data on the properties of alloys during irradiation is required. The alloy T-111 has been proved for use with lithium and potassium at high operating temperatures but little information is available on its properties during irradiation.

8. Neutronic Calculations

Tritium breeding ratios and the transmutation of the coolants (potassium and sodium) have been calculated for both overlayed and evaporator types of liquid-metal cooled lithium blankets, using a simplified model for neutron transport calculations. Nuclear heating rates in this specific model have not been calculated.

8.1 The Model

A one-dimensional cylindrical model has been used to reduce the problem to a size suitable for survey calculations. The materials in the blanket have been homogenized into a number of concentric annular regions, and a typical configuration is shown in table 4. The following approximations have been made:

a) The (natural) lithium - filled part of the cells has been homogenized into one region. This is an approximation because the cooling tubes are spaced to match the local heat input.

b) A uniform 14 MeV source has been used in the plasma region, thus the neutron current to the first wall is not thermally broadened and has an incorrect angular distribution.

c) TZM alloy has been treated as pure molybdenum. Of the alloying additions, titanium (0.5%) has several wide cross-section resonances and zirconium (0.1%) has a very low capture cross-section, but the error due to their neglect is small (< 2%). The neglect of zirconium in Nb-1Zr alloy also leads to an insignificant error (< 1%).

d) Inter-cell voidage and structural material have been ignored.

The neutron transport calculations were performed using the anisotropic scattering discrete ordinates code ANISN[17], employing 100 group nuclear data derived from ENDF/B-III[18]. The processes used to abstract the nuclear data are described in appendix J. Scattering matrices in the range P_o to P_8 were available, allowing a wide range of possible approximations.

The sensitivity of the calculations to the orders of quadrature and scatter was investigated (appendix K) and an S_8-P_1 approximation chosen. The mesh size was optimised and is indicated in table 4.

Calculations were performed for material volume fractions corresponding to wall loadings of 1, 5 and 10 MW/m^2 and for the wicked and one-through evaporator configurations. In addition, selected calculations were repeated using Nb-1Zr alloy instead of TZM as the structural material, sodium coolant instead of potassium, and with a two centimetre first wall. The volume fractions of the materials are given in table 5, and the corresponding number densities in table 6.

8.2 Tritium breeding ratios

The tritium breeding ratios (i.e. values normalised to one input neutron) are given for ^6Li, ^7Li and in total in table 8. These results are optimistic compared with those for a practical blanket design where allowance must be made for finite geometry, inter-cell voidage and streaming. For the case of optimum cylindrical cell packing, these factors have been calculated by Constantine et al[19] to lead to an approximate 6% reduction in tritium breeding ratios. In the present case the blanket density will be higher due to more efficient packing of the cells hence an error of 6% may be considered as an upper limit. The homogeneous approximation in the cell leads to inaccuracy because, in practice, the structure fraction is highest at the front of the cell, and because resonance self-shielding has been ignored. The latter applies particularly to the 900 barn resonance at 0.045 keV in molybdenum. To some extent these two effects self-cancel, but in the extreme case (once-through evaporator, TZM, 10 $MW.m^{-2}$) there are 0.4 captures in molybdenum for each input neutron so that the neutron balance is strongly influenced by changes in the effective structure cross-sections. However, even if the tritium breeding ratios are reduced by a total of 10% to allow for the above effects, and a further 5% is allowed for errors in the nuclear data[20], the lowest breeding ratio is 1.05. Allowing also for holes in the blanket (eg injectors and/or divertors) would probably reduce this figure to less than 1.0. In a practical design, the breeding ratio could be altered as required, either by changing the lithium inventory or isotopic ratio, or by altering the structure fraction.

The effects of possible changes in the cell configuration and structure are shown in table 8, for the most typical case (wicked configuration $5MW/m^{-2}$). Comparisons of cases 2 and 9 show that a 2 cm molybdenum first wall has a negligible effect (< 0.1%) while case 10 shows that the change to sodium coolant results in a small increase in breeding ratio (0.3%), due to the reduced thermal neutron absorption in sodium as compared

with potassium (case 2). The effect of replacing the TZM structural material by Nb-1Zr was investigated for the configurations of cases 2 and 6. The results are given in cases 7 and 8, and it is found that the tritium breeding ratios are reduced by 5% and 10% respectively. Thus the higher (n,2n) and lower capture cross-sections of molybdenum appear as a significant advantage when compared with niobium based alloys.

8.3 Transmutation in sodium and potassium

For all cases, the important reaction rates have been calculated for each material in the cell region and the neutron balances are shown in table 9, normalised to one input neutron. The discussion is limited to the transmutation in potassium and sodium, the structural materials having received more attention in the literature[21].

Table 9 shows that (n,γ), and (n,p) and (n,∝) reactions are all significant in potassium. Natural potassium consists of the two stable isotopes ^{39}K (93.1%) and ^{41}K (6.9%), with trace quantities of ^{40}K which may be considered stable for practical purposes. Thus, radiative capture in ^{39}K produces further stable isotopes, and only in ^{41}K does it lead to the production of an unstable isotope (^{42}K) which decays with a 12.5 hr half-life to ^{42}Ca. The (n,p) and (n,∝) reactions proceed as:

$$n + {}^{39}K \longrightarrow {}^{39}Ar + p$$
$$n + {}^{41}K \longrightarrow {}^{41}Ar + p$$
$$n + {}^{39}K \longrightarrow {}^{36}Cl + \alpha$$
$$n + {}^{41}K \longrightarrow {}^{38}Cl + \alpha$$

Of these products, ^{41}Ar (1.83 hr) and ^{38}Cl (37.3 min) decay quickly to ^{41}K and ^{38}Ar, and ^{39}Ar (265 yr) and ^{36}Cl (3.1×10^5 yr) are stable for practical purposes. Thus, the irradiation of potassium raises three problems:

a) Two of the products, helium and argon, are insoluble gases, and would have to be removed from the cooling circuit. Hydrogen would have to be removed to prevent diffusion into the cooling circuit structure.

b) Calcium and chlorine are chemically reactive and their inter-action with the materials in the cooling circuit (particularly the wicks) requires investigation in a detailed study.

c) The radioactive gaseous isotopes raise significant problems of containment and shielding.

These transmutations take place on a small scale, and to give an appreciation of their meaning they have been quantified in terms of production rates in a 5000 MW(th) reactor. The masses and equivalent volumes are given in table 10, and in calculating them it has been assumed that the short (< 1yr) half-lives are zero, the long (> 1yr) half-lives infinite, and that secondary transmutations are insignificant. In calculating hydrogen and helium quantities the (n,α), $(n,n')\alpha$, (n,p) and $(n,n')p$ reactions have all been included. The activities of the transmutation products are given in table 12, together with the radiation energies and intensities. The total activity of the structural material of most D-T fuelled reactor concepts is in the region of 10^6Ci/MW(th)[33], so the total sodium activity is relatively insignificant being only 3% of this amount. Also the radioactive products are all gaseous and a high proportion will be trapped and thence removed from the coldest part of the cooling circuit. Hence their presence will not cause a significant increase in the shielding requirements for the coolant ducts, but will necessitate the provision of a safe containment and storage facility which may be separated from the blanket/magnet area.

Transmutation in sodium (100% ^{23}Na) has been treated on the same basis, and again the (n,γ), (n,p) and (n,α) reactions are all considered. Radiative capture produces ^{24}Na which decays with a 15 hr half-life to ^{24}Mg (stable). The (n,p) reaction produces ^{23}Ne which decays rapidly (38 sec) to ^{23}Na, so this reaction has no net effect other than the production of hydrogen. The (n,α) reaction produces ^{20}F(11.2 sec) which decays to ^{20}Ne, which is stable. The quantities of hydrogen, helium, neon and magnesium produced in a reactor are detailed in table 11. The saturation activities of the unstable products are given in table 13. The total activity of these products would add approximately 25% to the radioactive inventory of a reactor, but most of this is due to short-lived gases which do not raise problems within the cooling circuit. However the ^{24}Na isotope is a significant γ-emitter and will be retained

in the cooling circuit, which may therefore require additional shielding at locations where it approaches radiation-sensitive components (e.g. the magnet coils) or where access is required.

8.4 Summary of neutronic calculations

The tritium breeding ratios obtained using an approximate model of a fusion reactor blanket are satisfactory, indicating that the use of potassium and sodium as blanket coolants raises no particular problems in this regard. The production of transmutations species in these coolants has been shown to occur on a significant scale, but the problems thus engendered are not likely to be severe.

9. THE USE OF SODIUM AS AN ALTERNATIVE TO POTASSIUM:

Sodium may be used as an alternative to potassium for fusion reactor blanket cooling. Its use, however, incurs both advantages and disadvantages. The higher latent heat of sodium (more than double that of potassium) permits lower sodium flowrates to each blanket cell for a given loading. This lower flowrate implies lower coolant velocity in the blanket cell and hence smaller MHD pressure losses in the primary circuit. For the potassium cooled cell, the stressing of the coolant ducts is the limiting factor so that it may be anticipated that the use of sodium would permit higher wall loadings than does potassium. However, as the reactor wall loading is increased the pressure drop increases sharply because both the coolant velocity increases and the magnetic field increases (if B_T is constant). The pressure drop in the primary coolant circuit is approximately proportional to the former quantity and to the square of the latter quantity. Moreover, at a given pressure in the boiling region, the saturation temperature of sodium is over 100°C higher than that for potassium. This has two important effects. It reduces the maximum permissible stress in the blanket structure (by lowering the yield stress and increasing creep rates) and it increases the problems of materials compatibility. Structure fraction of sodium will, therefore, be similar to that for potassium and restrictions on structure fraction will limit the reactor loading to a value of approximately 7 MW/m^2.

The breeding calculations presented in section 8 have shown that for a given geometry of cell, the breeding gain is slightly higher for sodium than for potassium. This is due to the lower absorption cross-section of sodium for thermal neutrons.

Figure 11 presents a graph of the maximum permissible wall loading for stress limitations in the cooling blanket of 25, 50 and 100 MN/m^2. If the maximum permissible stress is assumed to be 25 MN/m^2, a reactor wall loading of 5.5 MW/m^2 is permissible.

If the stress limit is increased to 50MN/m^2 a maximum reactor loading of 7 MW/m^2 is possible. Structure fraction does not approach its limiting value of 6% until the wall loading approaches the latter value. (refer appendix H)

A slightly higher reactor loading is, therefore, possible with sodium than with potassium but the structure temperatures in a sodium cooled cell are considerably higher than in a potassium cooled cell. Materials compatibility problems are already severe for a potassium cooled cell and will be critical for a sodium cooled cell.

In Appendix I, an analysis is given which shows that sodium is acceptable for use as a topping fluid for a sodium-steam turbine cycle. Comparison of figures 11 and 6 indicates that a slightly higher wall loading should be possible with sodium than potassium, however, its use may require considerable development of structural materials technology.

10. DISCUSSION:

The following factors have been examined in analysing the effectiveness of potassium and sodium for the present application:

1) Limitations set by stressing in the blanket structure. A brief indication of creep rates within the structure has been given.

2) Tritium breeding. A homogeneous model is applied to the blanket cells.

3) Reactor pumping power. Reactor pumping power greater than 2% of the reactor thermal output is considered as highly undesirable.

4) Structure fraction. A limitation of 6% on the structure fraction within the blanket region is imposed.

5) Lithium and structure temperatures have been evaluated. These define the severity of the materials compatibility requirements.

6) The compatibility of coolant, structure and lithium.

The following results have emerged:

a) Large volumes of liquid coolant (approx 20%) may be present in the cell and acceptable breeding ratios maintained by ~~modifying the lithium inventory~~.

b) Shaping of the boiling surfaces to ensure alignment with the dominant magnetic field is of great importance.

c) Research is required on the effect of longitudinal and transverse magnetic fields on critical heat flux and two phase pressure drop.

d) Because of the necessity to use structural alloys which are compatible with both lithium and potassium (or sodium) the use of materials which do not have a qualified metal industry is inevitable.

e) Wall loadings in excess of 7 MW/m² are difficult to achieve using available structural materials and alkali metal coolants. If, however, a means can be found of substantially reducing MHD pressure losses in the primary cooling circuit, the above figure may be exceeded.

f) Limitations on tritium breeding, stressing in the structure, structure-faction and pumping power, ~~independently yield~~ restrict the range of operation wall loadings ~~in the narrow range~~ 5-7 MW/m². ~~The narrowness of this band indicates that the design of the potassium cooled cell given above is near optimum in its basic parameters.~~

The limitation on stressing of the structure is the most severe of these restrictions.

11. CONCLUSIONS

This report is an examination of the effectiveness of potassium and sodium as indirect coolants for a fusion reactor blanket. It has been found that:

a) A calculated maximum wall loading of 5-7 MW/m^2 is permissable. On a strictly comparable basis, this is higher than the loading possible with a direct lithium cooled blanket and is similar to that achievable in an indirect helium cooled blanket.

b) The most severe limitation is that of the stressing of the duct walls, though at a wall loading of 5-7 MW/m^2, many other parameters (structure fraction, breeding ratio, structure and lithium temperatures) are also approaching their limiting values. There will be a certain location within the blanket structure where the combination of radiation damage, temperature and pressure give rise to the limiting stressing or largest creep rate. In a more detailed analysis of blanket design, emphasis would be given to determining such a location.

c) By limiting the velocity of the potassium vapour in the coolant ducts, it is possible to operate a potassium cooled cell at a pressure of several bars in the zones of highest radiation damage. This is necessary to maintain the temperature in the boiling region at as low a level as possible.

d) The temperature levels in a potassium cooled blanket (900° - 1000°C) permit thermal efficiences for power producing cycles in excess of 50%[23].

e) Potassium technology is sufficiently advanced (e.g. the space programme) that standards for safety and design are currently available.

f) Potassium loses its advantages as a fusion reactor coolant at low wall loadings (≤ 1 MW/m^2) because efficient use is not made of the high heat transfer coefficients characterstic of boiling liquid metals.

g) A breeding blanket of radial thickness 1 metre is sufficient to provide a breeding gain in excess of 1.2, if required.

h) In order to limit the MHD induced stressing of the structure, coolant ducts must be as large as possible. As the coolant supply ducts are enlarged, however, structure fraction increases and breeding gain decreases. The optimised potassium cell is a compromise between these conflicting requirements.

i) The configuration of cell in which wick overlayed plates are used for evaporating the potassium appears (from heat transfer and pressure drop considerations) to be preferable to the conventional boiling tube arrangement.

These findings indicate that potassium is attractive for use as a coolant for a fusion reactor blanket. It does, however, possess several disadvantages:

1) The operating temperature ~~(1103 K)~~ (830°C) for a potassium cooled blanket cell sets severe problems of corrosion of structural materials. The complexity of the potassium cooled cell would necessitate long operational lifetimes. Little published data currently exists on the compatibility of structural materials with both lithium and potassium over long periods. There is also a lack of corresponding data on material properties and radiation damage.[22]

2) Economic considerations. The capital cost of alkali metal circuitry and plant is likely to be high but possibly matched by the high efficiency of the power plant.[23]

3) For the overlayed boiling surfaces arrangement, there is a possibility of the deposition of particles and oxide in the porous structure. This might result in a steady deterioration of the heat transfer characteristics of the wick and a reduction of the reactor rating.

4) Purity of the potassium coolant must be maintained at high levels to limit corrosion and deposition in the wicked surfaces.

5) The coolant flow may distort the magnetic field in the vicinity of the cooling ducts. This might lead to the formation of secondary induced fields and may marginally increase the problems of plasma containment.

6) The complexity (and/the cost (pressurizing)) of potassium cooled blanket cells is greater than that for direct lithium cooling, though it is comparable with that of a helium cooled cell.

7) To obtain uniform distribution of liquid potassium to the overlayed surfaces great care is required in arranging suitable arteries. Little developmental work in this area is available in the published literature.

8) Neutron-induced transmutation reactions result in the presence of impurities in the coolant. The interaction of

these impurities with the materials of the cooling circuit requires investigation.

g) The levels of radioactivity in the circuit would be significant. It would be necessary to provide for the removal of radioactive gases, and in a sodium circuit the presence of the ^{24}Na isotope would necessitate the provision of additional shielding.

An engineering concept of an alkali-metal cooling system for a cellular fusion reactor blanket has been described. The overall feasibility of this method of blanket cooling has been demonstrated and the principle design features of the system have been outlined. The use of sodium leads to a potentially higher reactor wall loading than is possible using potassium but incurs a higher temperature level in the blanket. This increases structural creep rates and reduces blanket operational lifetime. ~~The~~ because of this increased structure temperature use of potassium appears to be preferable within the limitations set by current materials technology.

Much work remains to be done, but the potassium cooling arrangement shows promise for use in ~~commercial~~ fusion reactors where high wall loading is required. ~~It is also felt that a potassium cooling loop~~ The maximum wall loading that can be achieved with a potassium or sodium coolant is ~~similar~~ apparently similar to that ~~of a helium~~ which is possible with a helium coolant. ~~In addition~~ A considerably greater depth than is possible here is required before the ~~relative~~ merits of the coolant can be ~~fully~~ stated.

Acknowledgements

The authors gratefully acknowledge the assistance and advice of J.T.D. Mitchell, Culham Laboratory, J.G. Collier of Chemical Engineering Division, Harwell and Dr. J.C. Hunt of Cambridge University.

TABLE 1

Main Reactor Parameters	$\eta = 0.32$; $A_\omega = 4.60$; $A_p = 6$			
Reactor Electrical Output	2500	2500	2500	(MW)
Thermal Wall loading	1	5	10	(MW/m^2)
Major radius of Torus	31	13.9	9.8	(m)
Minor radius of Torus	6.4	2.87	2.02	(m)
Length of cell, reflector and Shielding	1.8	1.8	1.8	(m)
Inner magnet surface radius	8.2	4.67	3.82	(m)
Length through magnets	1.0	1.0	1.0	(m)
Maximum magnetic field intensity	7	14	19	tesla

TABLE 2

CHOICE OF BLANKET MATERIAL FOR SHORT TERM POWER PLANT WITH POTASSIUM COOLANT (adapted from reference 16)

Decreasing Importance ↓

Property	First Choice	Second Choice
Qualified Metal Industry	TZM	Nb-1Zr
Fabricability, weldability	Nb-1Zr	TZM
Radiation damage embrittlement	?	?
Swelling Resistance	TZM	Nb-1Zr
Sputtering and blistering	Nb-1Zr	TZM
Interstitial embrittlement	TZM	Nb-1Zr
Allowable operating temperature	TZM	Nb-1Zr
Effect on breeding ratio	Nb-1Zr	TZM
Fabrication costs	Nb-1Zr	TZM

(16,22)

(a) only the non-magnetic alloys Nb-1Zr and TZM are considered.

(b) all alloys allow breeding, the question here is the value of the doubling time.

TABLE 3

Structure and Lithium Temperatures - wall loading = 7.5 MW/m²

location	potassium temp (°K)	tube wall ΔT	Structure ΔT from vol. heating.	Structure ΔT from rod heating.	Lithium Δt vol. and transfer heating.	max temp. tube (°K)	max temp. cell wall (°K)	max temp. lithium (°K)
at front wall of cell	1110 (1)	7.6 (2)	44 (3)	56 (4)	-	1118	1218	-
midway between cooling channels near front of cell	1110 (1)	7.6 (2)	30 (5)	10 (6)	-	1113	1158	-
midway between cooling channels at rear of the cell	1110 (1)	7.6 (2)	-	-	205	1113	-	1323
boundary of cell not exposed to direct shine of plasma	1110 (1)	7.6 (2)	-	-	62	1118	-	1180

(1) common to all locations
(2) for 20 plates of thickness 0.2 cm
(3) midway between plate and 7mm wall
(4) Bremsstrahlung = 0.05 P_w
(5) midway between tubes and for 5mm wall
(6) Bremsstrahlung = 0.01 P_w
(7) Structure Fraction ≈ 0.06

Table 4. Configuration of Neutronic Calculations

	PLASMA	VOID	CELL	REFLECTOR
Zone No.	1	2	3	4
Materials	-	-	Potassium Lithium Structure	Graphite
Source	14 MeV Uniform Isotropic	-	-	-
Thickness (cm)	150	50	100	25
Intervals	-	-	25	5

Note

1) The mesh intervals were of equal thickness within each region.

2) An albedo of zero was applied to the outer boundary of the reflector region.

Table 5. Cell volume fractions for Neutronic Calculations

CASE	STRUCTURE	COOLANT	LITHIUM	VOIDAGE
Wicked, 1 $MW.m^{-2}$	0.0320	0.1150	0.8402	0.0128
" , 5 $MW.m^{-2}$	0.0590	0.1391	0.7778	0.0241
" ,10 $MW.m^{-2}$	0.0940	0.1501	0.7183	0.0376
Once-through evaporator, 1 $MW.m^{-2}$	0.0354	0.1171	0.8334	0.0141
" " " 5 $MW.m^{-2}$	0.0744	0.1451	0.7496	0.0309
" " " 10 $MW.m^{-2}$	0.1220	0.1632	0.6640	0.0508

Notes:

1) The only voidage taken into account is that in the cooling circuit. The small quantity of coolant vapour has been added to the coolant fractions.

2) The reflector was taken to be 100% graphite, and the first wall to be 100% structure.

Table 6. material number densities for Neutronic Calculations

CASE NO	DESCRIPTION	Number Densities for Cell Region (atoms.cm^{-3} x10^{24})					
		Li^6	Li^7	Mo	Nb	K	Na
1	Wicked, TZM, 1MW.m^{-2}	0.0028891	0.0360466	0.0020086		0.0015234	
2	" " 5MW.m^{-2}	0.0026745	0.0333695	0.0037033		0.0018426	
3	" " 10MW.m^{-2}	0.0024699	0.0308168	0.0059002		0.0019883	
4	OTEC(1), TZM, 1MW.m^{-2}	0.0028657	0.0357549	0.0022220		0.0015512	
5	" " 5MW.m^{-2}	0.0025775	0.0321597	0.0046699		0.0019221	
6	" " 10MW.m^{-2}	0.0022832	0.0284872	0.0076577		0.0021618	
7	Case 2 with Nb-1Zr structure	0.0026745	0.0333695		0.0032508	0.0018426	
8	Case 6 with Nb-1Zr structure	0.0022832	0.0284872		0.006722C	0.0021618	
9	First Wall (See Note 2)	0.0026745	0.0333695	0.0037033		0.0018426	
10	Sodium Cooling (see Note 3)	0.0026745	0.0333695	0.0037033			0.0035347

Notes:

1) Once-through evaporator configuration.
2) The first wall consisted of 2cm of molybdenum with number density 0.0627681, otherwise as case 2.
3) All other data as for case 2
4) For all cases the reflector was pure graphite, number density 0.080385.

Table 7. Tritium breeding ratios for various Neutron Transport Approximations

Note:

These ratios apply to the case of a wicked cell with TZM structure and 5 MW/m^2 wall loading.

ORDER OF ANGULAR QUADRATURE	ORDER OF SCATTER	^6Li TRITIUM BREEDING RATIO	^7Li TRITIUM BREEDING RATIO	TOTAL TRITIUM BREEDING RATIO
S_4	P_0	0.9036	0.5984	1.502
S_6	P_0	0.9029	0.5984	1.501
S_6	P_1	0.8868	0.5944	1.481
S_8	P_1	0.8866	0.5943	1.481
S_8	P_3	0.8839	0.5927	1.477
S_{12}	P_3	0.8838	0.5926	1.476

Table 8. Summary of Tritium Breeding Results

CASE NO.	$^6Li(n,\alpha)t$	$^7Li(n,n'\alpha)t$	TOTAL t
1	0.917	0.696	1.613
2	0.887	0.594	1.481
3	0.849	0.495	1.344
4	0.914	0.683	1.597
5	0.870	0.547	1.417
6	0.808	0.425	1.233
7	0.820	0.584	1.404
8	0.714	0.407	1.121
9	0.887	0.593	1.480
10	0.910	0.575	1.485

Notes:

1) Results normalised to one input neutron.

2) Case numbers defined in table 6.

e 9. Neutron reactions for cell region

REACTION	CASE NO.									
	1	2	3	4	5	6	7	8	9	10
o (n,2n)	0.0855	0.1504	0.2235	0.0940	0.1841	0.2758			0.1501	0.1456
o absorption	0.1033	0.1918	1.3060	0.1142	0.2424	0.3987			0.1919	0.2052
b (n,2n)							0.1095	0.2046		
b absorption							0.2187	0.4238		
b (n,p)							0.0037	0.0066		
b (n,α)							0.0010	0.0019		
(n,2n)	0.0001	0.0001	0.0001	0.0001	0.0001	0.0001	0.0001	0.0001	0.0001	
n,n')α	0.0013	0.0016	0.0016	0.0013	0.0016	0.0016	0.0016	0.0017	0.0016	
absorption	0.0542	0.0619	0.0621	0.0548	0.0625	0.0640	0.0587	0.0575	0.0618	
n,γ)	0.0072	0.0090	0.0099	0.0075	0.0094	0.0108	0.0079	0.0086	0.0089	
(n,n')p	0.0099	0.0114	0.0114	0.0101	0.0115	0.0117	0.0115	0.0119	0.0114	
n,p)	0.0351	0.0397	0.0393	0.0354	0.0399	0.0403	0.0381	0.0369	0.0397	
n,α)	0.0119	0.0132	0.0129	0.0119	0.0132	0.0131	0.0127	0.0120	0.0132	
a (n,2n)										0.0017
a absorption										0.0299
a (n,γ)										0.0033
a (n,p)										0.0083
a (n,α)										0.0183
(n,2n)α	0.0071	0.0062	0.0054	0.0070	0.0058	0.0047	0.0063	0.0048	0.0062	0.0061
Li absorption	0.9191	0.8885	0.8503	0.9163	0.8722	0.8091	0.8218	0.7150	0.8890	0.9118
(n,p)	0.0022	0.0019	0.0016	0.0021	0.0017	0.0014	0.0017	0.0012	0.0019	0.0018
Li ,α)t	0.9169	0.8866	0.8487	0.9142	0.8704	0.8077	0.8201	0.7138	0.8871	0.9099
(n,2n)	0.0277	0.0245	0.0211	0.0273	0.0229	0.0185	0.0246	0.0187	0.0244	0.0237
(n,2n)α	0.0333	0.0300	0.0263	0.0329	0.0283	0.0235	0.0301	0.0238	0.0299	0.0291
Li absorption	0.0113	0.0101	0.0089	0.0111	0.0095	0.0079	0.0101	0.0079	0.0100	0.0098
(n,α)	0.0108	0.0097	0.0084	0.0107	0.0091	0.0075	0.0097	0.0076	0.0096	0.0094
Li (n,n'α)t	0.6962	0.5944	0.4950	0.6832	0.5473	0.4246	0.5841	0.4068	0.5934	0.5753

e:

ese results are normalised to one input neutron.

Table 10. Transmutation products in potassium

	Mass (gms)	Volume at N.T.P. (gases only)(litres)
Hydrogen	1.15	12.84
Helium	1.33	7.41
Argon (^{38}Ar + ^{39}Ar)	33.8	19.0
^{36}Cl	10.5	3.3
^{42}Ca	0.024	-
	total mass = 46.3 (gms)	total volume = 42.55 litres

Table 11. Transmutation products in sodium

	Mass (gms)	Volume at N.T.P. (gases only)(litres)
Hydrogen	0.19	2.1
Helium	1.64	9.2
^{20}Ne	8.3	9.2
^{24}Mg	1.8	-
	total mass = 11.93 (gms)	total volume = 20.5 litres

Notes for tables 10 and 11:

a) Quantities are derived for 1 day of operation of a 5000 MW(th) reactor, assuming total energy release of 20 MeV per fusion.

b) Short half-lives have been taken as zero, long ones as infinite (see text).

c) Secondary reactions have been ignored.

d) The results apply to the wicked cell configuration rated at 5 $MW.m^{-2}$ with TZM structure.

Table 12 ACTIVITY IN IRRADIATED POTASSIUM

ISOTOPE	HALF-LIFE	ACTIVITY (CURIES)	β-RAY ENERGIES (MeV) AND INTENSITIES (%)	γ-RAY ENERGIES (MeV) AND INTENSITIES (%)
^{39}Ar	265 yr	$4.08 \cdot 10^{5}$ (Annual increase)	0.565 max (100%)	-
^{36}Cl	$3.1 \cdot 10^{5}$ yr	$1.16 \cdot 10^{2}$ (Annual increase)	0.714 max (98%)	-
TOTAL		$4.08 \cdot 10^{5}$ (Annual increase)		
^{41}Ar	1.83 hr	$1.16 \cdot 10^{8}$ (Saturated)	2.49 max (0.8%) 1.198 max (99.2%)	1.293 (99.2%)
^{38}Cl	37.3 min	$3.84 \cdot 10^{7}$ (Saturated)	4.91 max (53%) 2.74 max (9%) 1.14 max (38%)	2.17 (47%) 1.6 (38%)
TOTAL		$1.54 \cdot 10^{8}$ (Saturated)		

Table 13 ACTIVITY IN IRRADIATED SODIUM

ISOTOPE	HALF-LIFE	ACTIVITY (CURIES)	β-RAY ENERGIES (MeV) AND INTENSITIES (%)	γ-RAY ENERGIES (MeV) AND INTENSITIES (%)
^{24}Na	15 hr	$1.40 \cdot 10^{8}$ (Saturated)	1.389 max (99%)	2.754 (100%) 1.369 (100%)
^{23}Ne	38 sec	$3.49 \cdot 10^{8}$ (Saturated)	4.38 max (67%) 3.94 max (32%) 2.30 max (0.9%)	1.64 (0.9%) 0.439 (32.9%)
^{20}F	11.2 sec	$7.70 \cdot 10^{8}$ (Saturated)	5.41 max (100%)	1.63 (100%)
TOTAL		$1.26 \cdot 10^{9}$ (Saturated)		

Notes for Tables 12 and 13

a) Activities are calculated for a 5,000 MW(th) reactor, assuming a total energy release of 20 MeV/fusion.

b) The results apply to the wicked cell configuration rated at $5 MW\text{-}m^{-2}$ with TZM structure.

REFERENCES

1. HUNT, J.C.R. and HANCOX R., "The Use of Liquid Lithium as Coolant in in a Toroidal Fusion Reactor - Part I, Calculations of Pumping Power", Culham Laboratory Report CLM-R115 (1971)

2. HANCOX R. and BOOTH J.A."The Use of Liquid Lithium as Coolant in a Toroidal Fusion Reactor - Part II, Stress Limitations", Culham Laboratory Report CLM-R116(1971)

3. MITCHELL, J.T.D. and BOOTH J.A. "Wall Loading Limitations in a helium cooled Fusion Reactor Blanket", Culham Laboratory Report CLM-R126, (1973).

4. MITCHELL, J.T.D. and HANCOX R., "A Lithium Cooled Toroidal Fusion Reactor", Paper presented at the Intersociety Energy Conversion Engineering Conference, San Diego, U.S.A. 25-29 September, 1972.

5. MITCHELL, J.T.D. and GEORGE, M.W. "A design concept for a Fusion Reactor Blanket and Magnet Shield Structure", U.K.A.E.A. Culham Laboratory Report CLM-R 121, (1972).

6. STANBRIDGE, J.R. CARRUTHERS, H.M. KEEN B.A., and SHOTTER H.A. "Design of Stainless Steel Blanket Cells for a Fusion Reactor" U.K.A.E.A. Culham Laboratory Report CLM-R 127 (1974).

7. OWEN, R.G. HUNT, J.C. and COLLIER, J.G. "Magnetohydrodynamic pressure drop in ducted two-phase flows" to be published as a preprint of the U.K.A.E.A. Culham Laboratory.

8. FRASS, A.P. LLOYD, D.B. and MacPHERSON, R.E. "Effect of alkali metals (lithium, sodium, potassium) OAK RIDGE NATIONAL LABORATORY REPORT ORNL-TM-4213 (Feb 1973)

9. BLOW, S. Private Communication, 1972.

10. PARKIN, J.R. SCHMIDT, P.S. and VLIET, G.G. "Design of a boiling potassium heat removal system for fusion reactors". Symposium on the Technology of controlled nuclear fusion, San Diego 16-18 April 1974, Vol. 1 p664-676.

11. ROSSENBLUM, L. et al. "Potassium Rankine System Material Technology", Space Power Systems Advanced Technology Conference, SP 131, (1966) NASA pp 169-199.

12. FRANK, R.G. et al. "Material and Process Specifications for Refractory Alloy and Alkali Metals", G.E. Report R66SD3007 (1965).

13. HARRISON, R.W. and HOFFMAN, E.E. "Advanced Refractory Alloy Corrosion Loop Program, Quarterly Progress Report No. 11 for quarter ending January 15th, 1968", NASA CR-72383, (1968) Contract NAS3-6474 Space Power and Propulsion Sec., General Electric Co.,

14. MOSS, T.A. DAVIES R.L. and MOORHEAD, P.E. "Material Requirements for Dynamic Nuclear Space Power Systems". Winter Meeting of the American Society of Mechanical Engineers, Pittsburgh, Pa. 1967, also TMX-52344, 1967, NASA.

15 MANSON, S.V. "A Review of the alkali Metal Rankine Technology Program", Journal of Spacecraft and Rockets, vol. 5, No. 11, November, 1968.

16 MAYNARD, C.W. and FORSEN, H.K. "University of Wisconsin Fusion Design Studies", University of Wisconsin Report, Madison Wisconsin (1972).

17 ENGLE, W.W. "A User's Manual for ANISN"; Oak Ridge National Laboratory RSIC report K-1639 (March, 1967).

18. DRAKE, M.K. (ed.). "Data Formats and Procedures for the ENDF neutron cross-section library", BNL-50274 (T-601) (October, 1970).

19 CONSTANTINE, G, et al "Neutronics of Cellular Blankets for Fusion Reactors:- CLM-R136 (May, 1975).

20. STEINER, D, TOBIAS, M, "Cross-section sensitivity of tritium breeding in a fusion reactor blanket", Nuclear Fusion 14, 153-163 (1974).

21 "Proceedings of the 2th symposium on Fusion Technology" June 17-21, 1974 sections E3, E4, Euratom report EUR 5182e

22 DRALEY, K.E. FROST B.R.T., GRUEN, D.M. KAMINSKY, M. and MARONI, V.A., "An Assessment of some materials problems for Fusion Reactors", Intersociety Energy Conversion Engineering Conference 1971.

23. COLLIER, J.G. and COX, R.F., and EVANS L.S. "A Potassium-steam binary turbine cycle for a high temperature gas cooled reactor", U.K.A.E.A. Report A.E.R.E. R7038 (1972).

24. MITCHELL, J.F.D. and BOOTH J.A., "Wall Loading and Structure Cooling in Fusion Reactor Blankets based on Pumped Lithium Heat Transport", Technology Support Group Report 1971, U.K.A.E.A. Culham Laboratory.

25. MACBETH, R.V. "Boiling on Surfaces Overlayed with Porous Deposit: Heat Transfer Rates obtained by Capillary Action", UKAEA Report AEEW-R711 (1971).

26. SIMINOV, G.F. and MISHCHENKO, L.N, "Procedure for Selection of Geometrical Parameters of Low Temperature Heat Pipes", Therm, Eng. Vol. 20, No 8, pp 114-117, August, 1973.

27 CHISHOLM, D. "The Heat Pipe", M & B Technical Library TL/ME/2, Mills and Boon Ltd. (1971).

28 KUNZ, H.R, LANGSTON, L.S, HILTON, B.H, WYDE, S.S. and NASHICK, G.H. "Vapour-Chamber Fin Studies - Transport Properties and Boiling Characteristics of Wicks" NASA Report CR-812. 1967.

29 COLLIER, J.G. "Boiling of Liquid Alkali Metals", CPE-Heat Transfer Survey (1968).

30. OAK RIDGE NATIONAL LABORATORY. RSIC data library collection DLC-2/100G.

31. WRIGHT, R.Q. et al. "SUPERTOG. A program to generate fine group constants and P_n scattering matrices from ENDF/B", ORNL-TM-2679 (September, 1969).

32. CONSTANTINE, G. Private communication (1974).

33. CONN, R.W, SUNG, T.Y, ABDOU, M.A. "Comparitive study of radioactivity and afterheat in several fusion reactor blanket designs." University of Wisconsin report UWFDM-113 (1974)

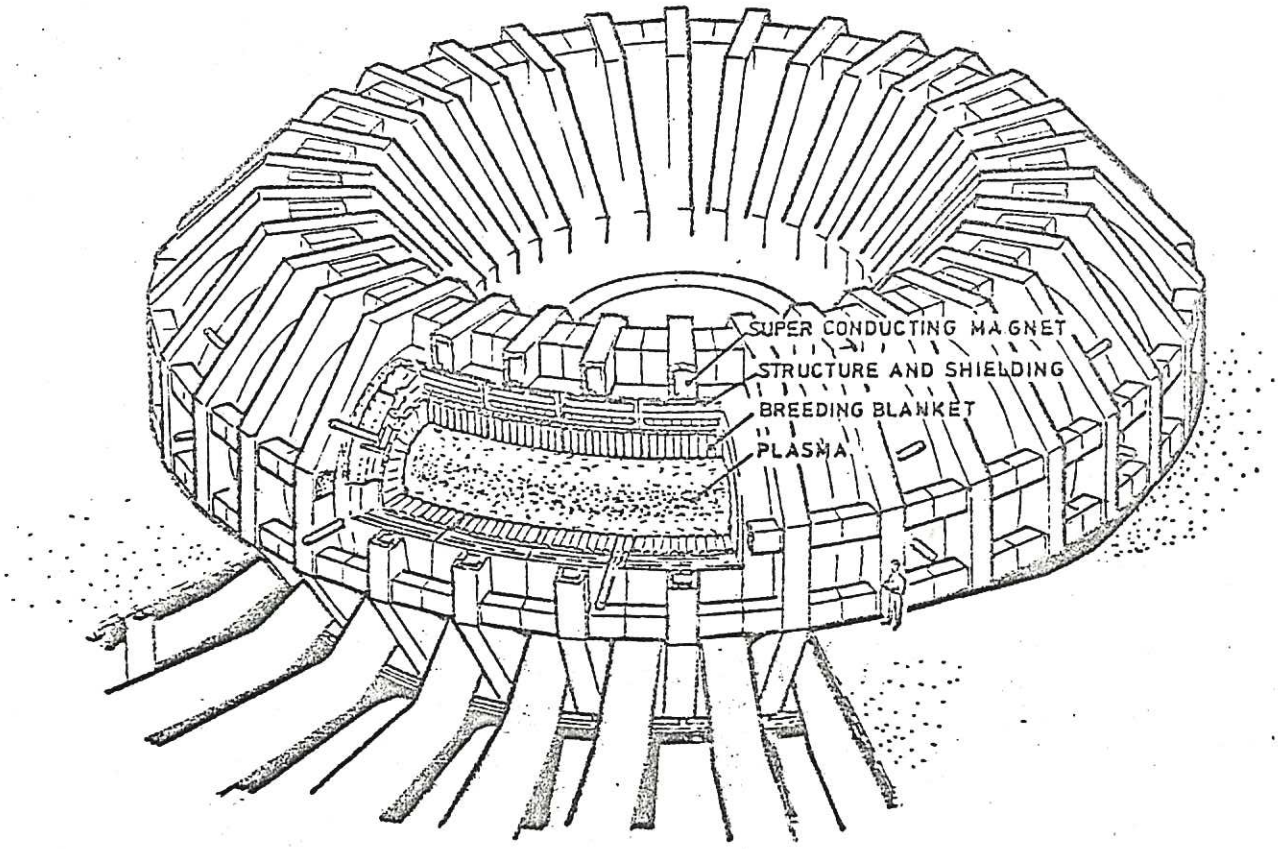

FIGURE 1. GENERAL VIEW OF A TOROIDAL FUSION REACTOR

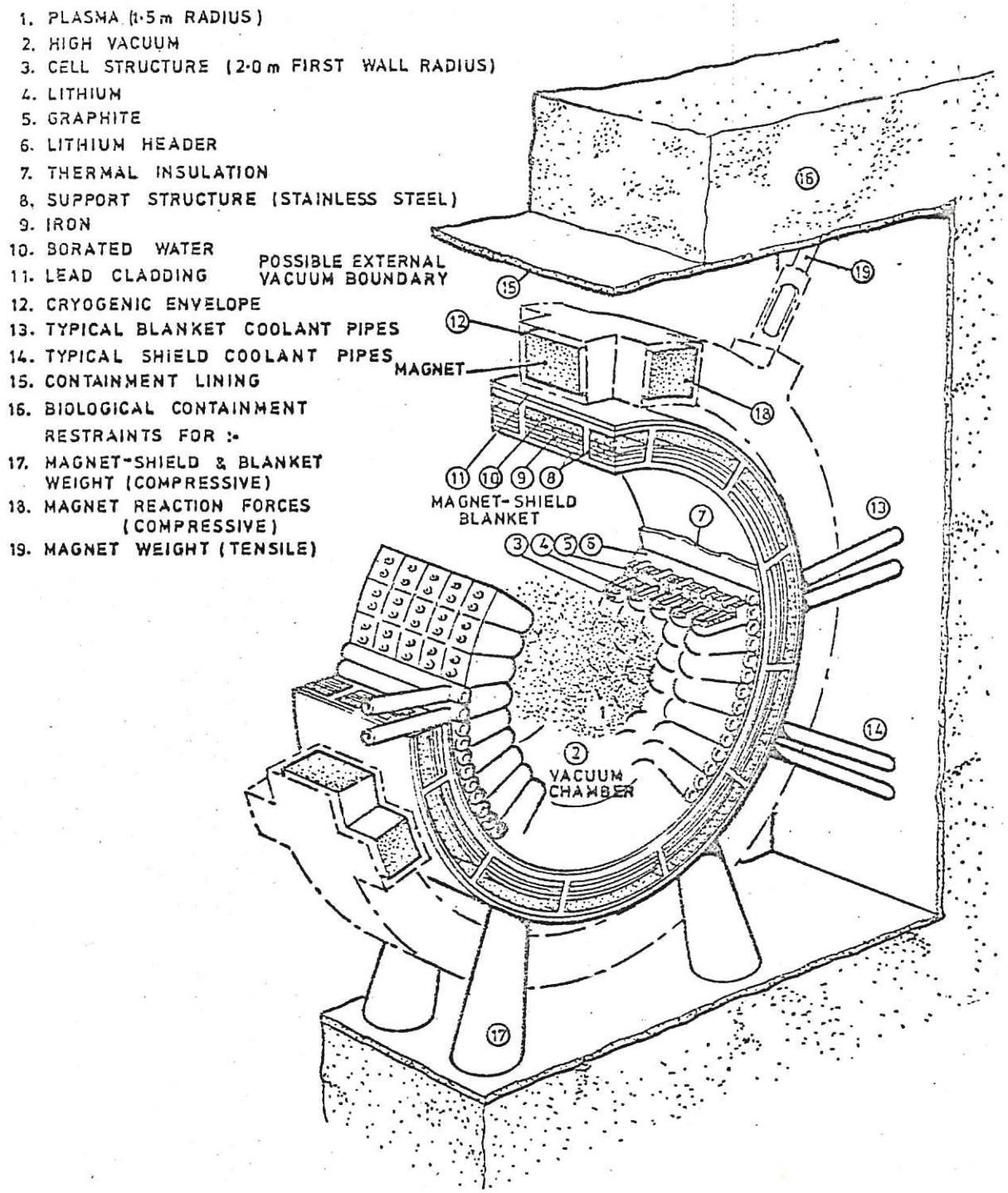

FIGURE 2. FUSION REACTOR PLASMA CONTAINMENT-GENERAL ARRANGEMENT

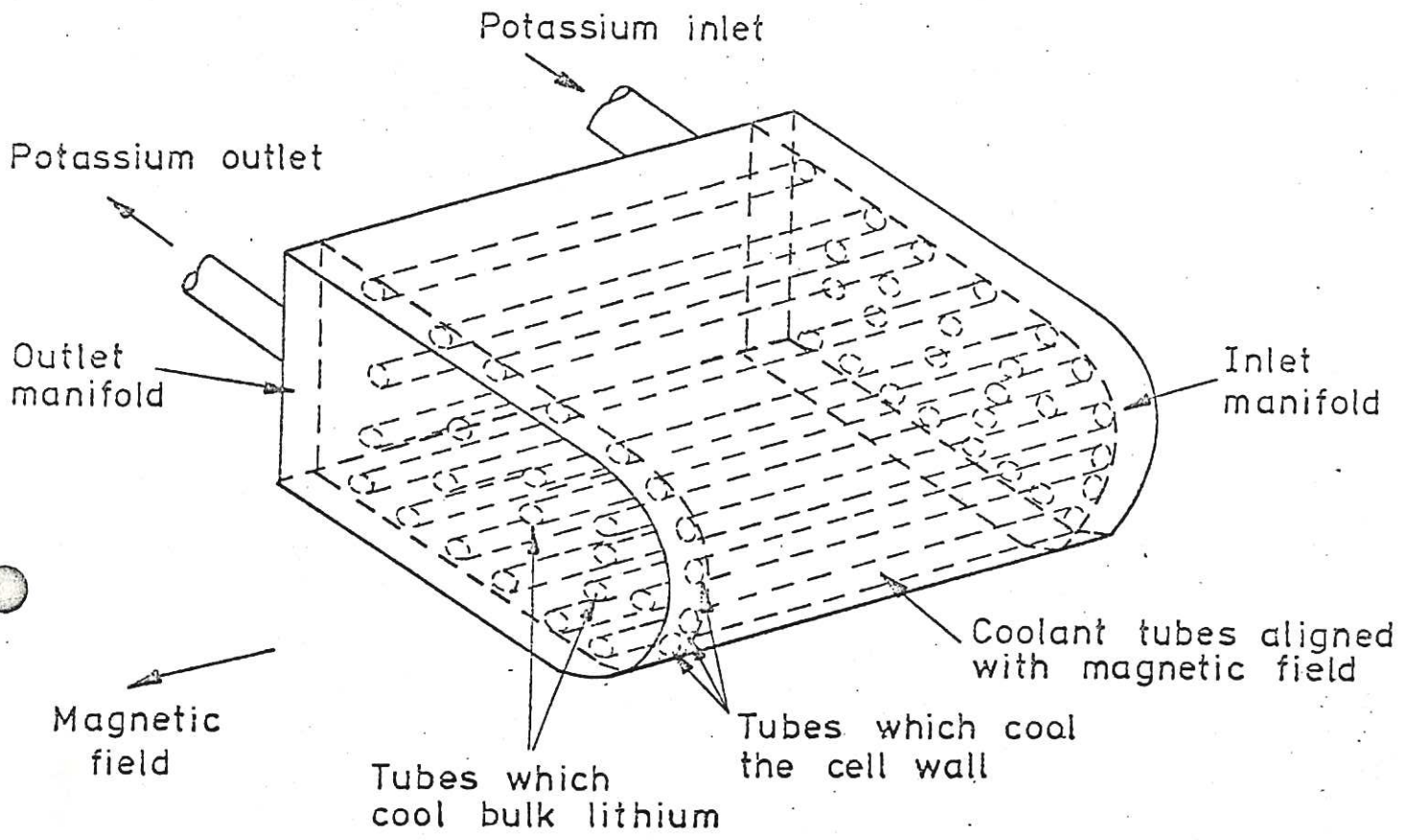

FIG. 3. A FUSION REACTOR BLANKET CELL FOR TWO-PHASE POTASSIUM COOLING - ONCE THROUGH EVAPORATOR CONFIGURATION.

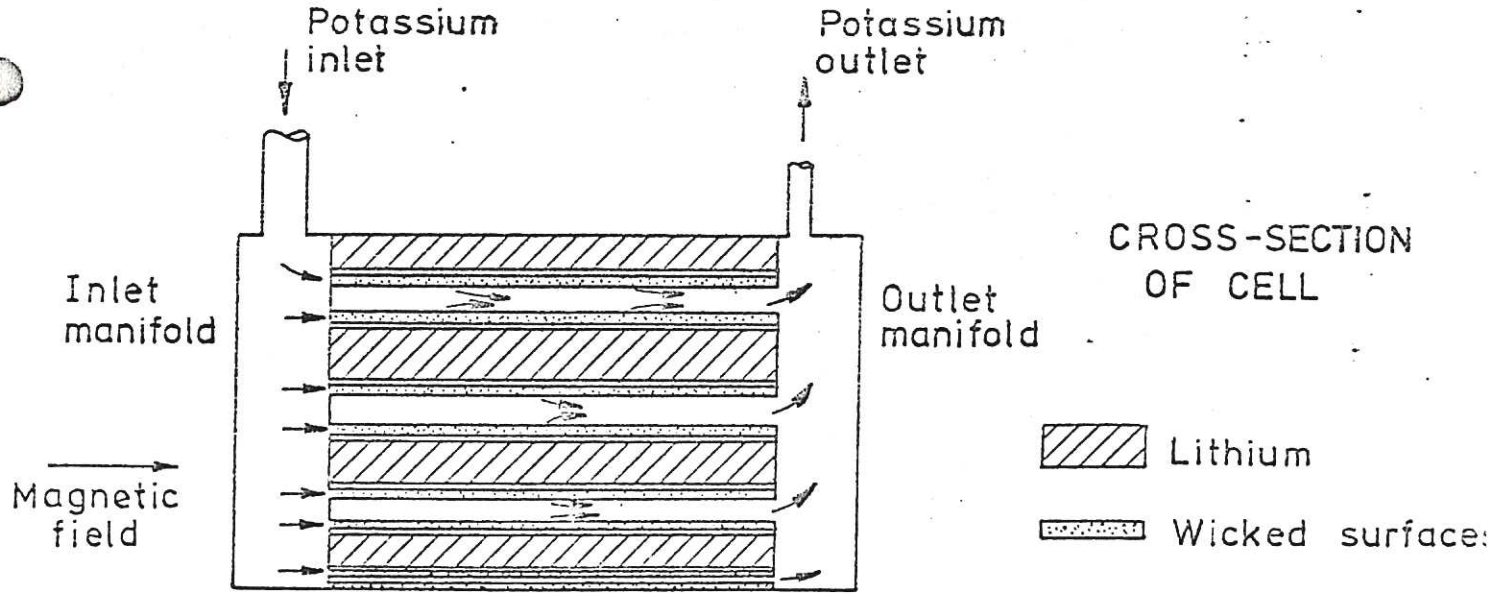

FIG. 4. A FUSION REACTOR BLANKET CELL FOR TWO-PHASE POTASSIUM COOLING - WICKED CONFIGURATION.

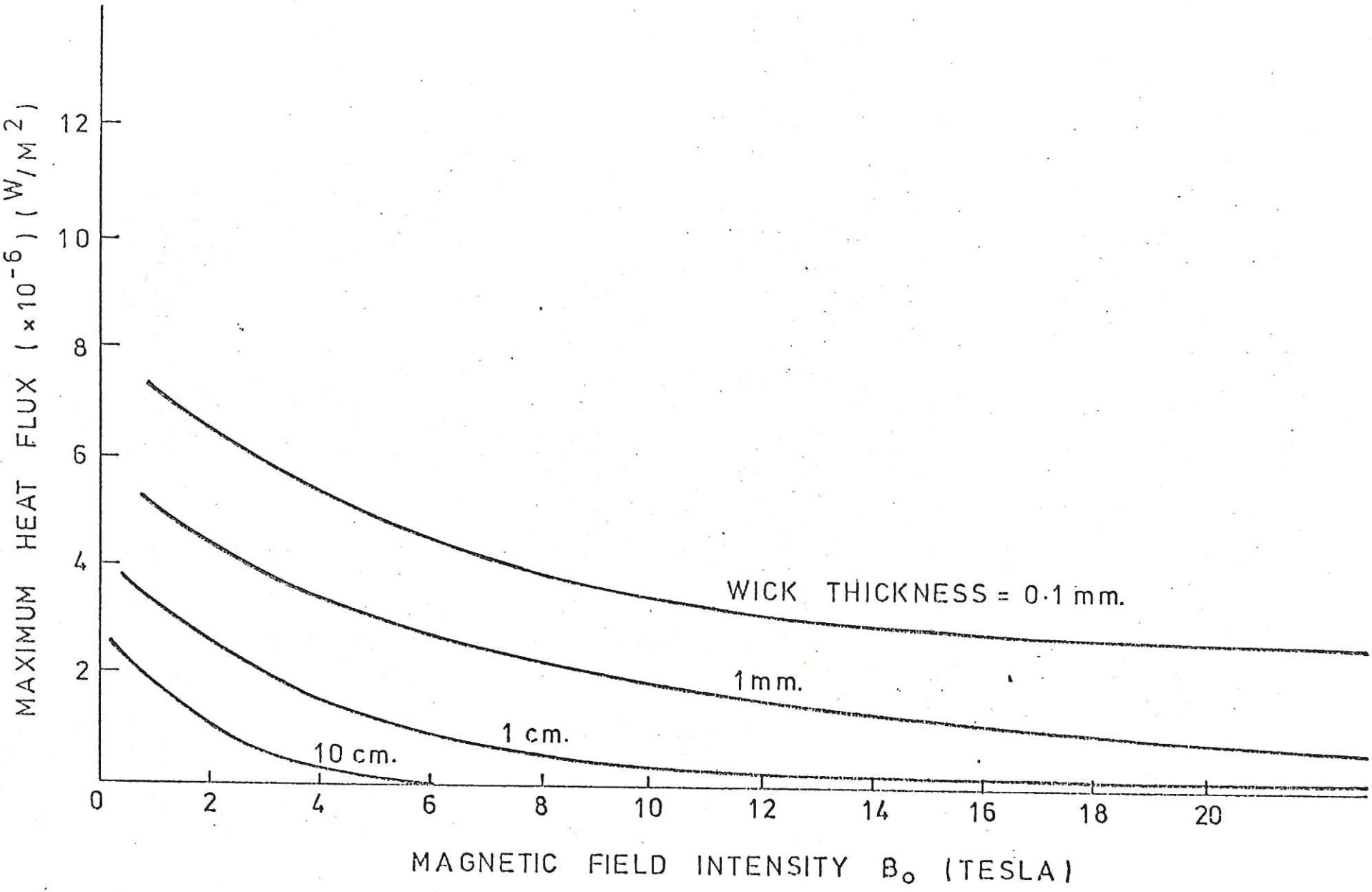

FIG. 5 CURVES OF MAXIMUM HEAT FLUX AS A FUNCTION OF MAGNETIC FIELD INTENSITY FOR POROUS WICKS OF VARIOUS THICKNESS.

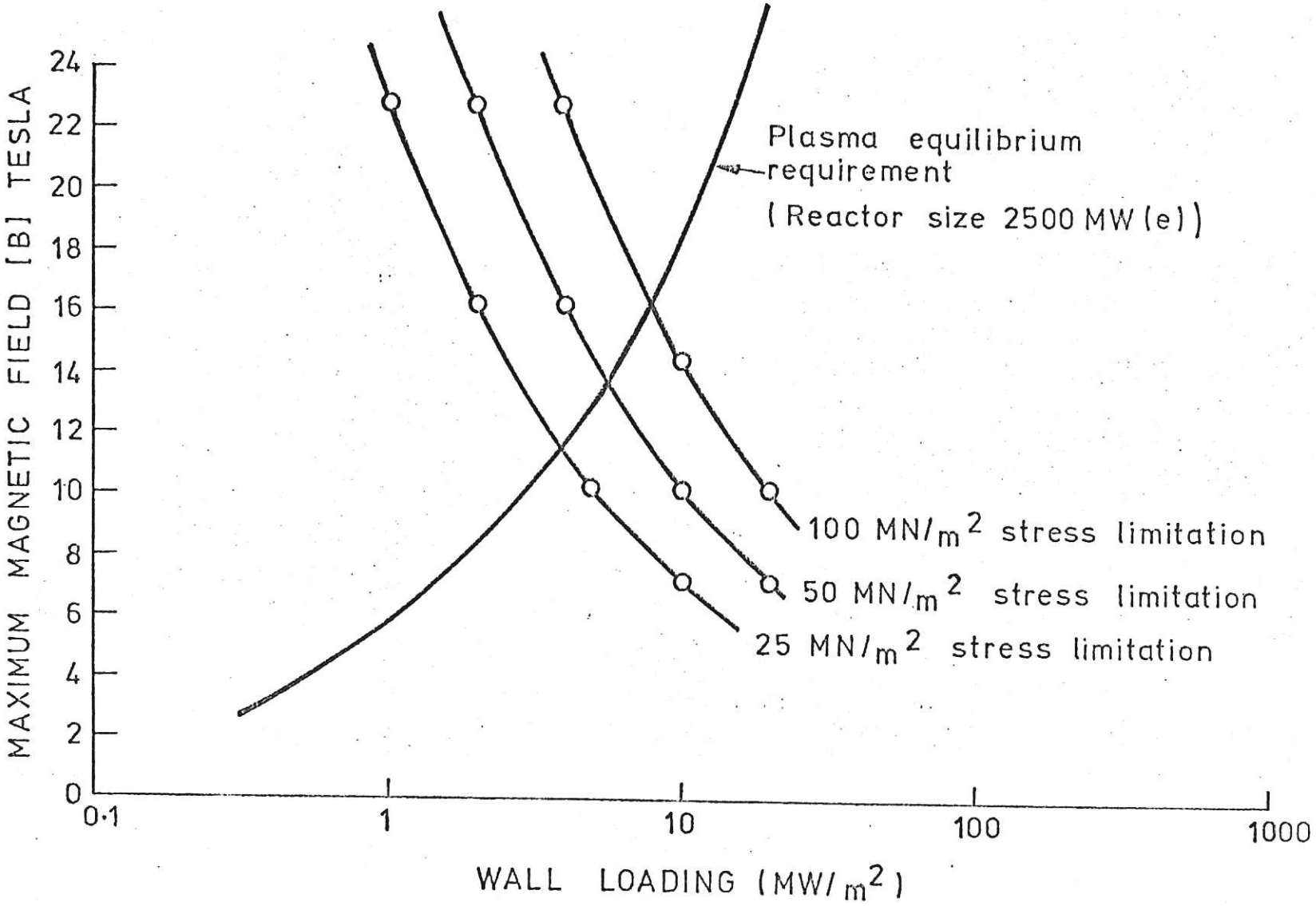

FIG. 6. LIMITATIONS ON REACTOR FIRST WALL LOADING IMPOSED BY STRESSING OF A POTASSIUM COOLED BLANKET. CURVES ARE GIVEN FOR MAXIMUM STRESS LEVELS OF 100, 50 AND 25 MN/m²

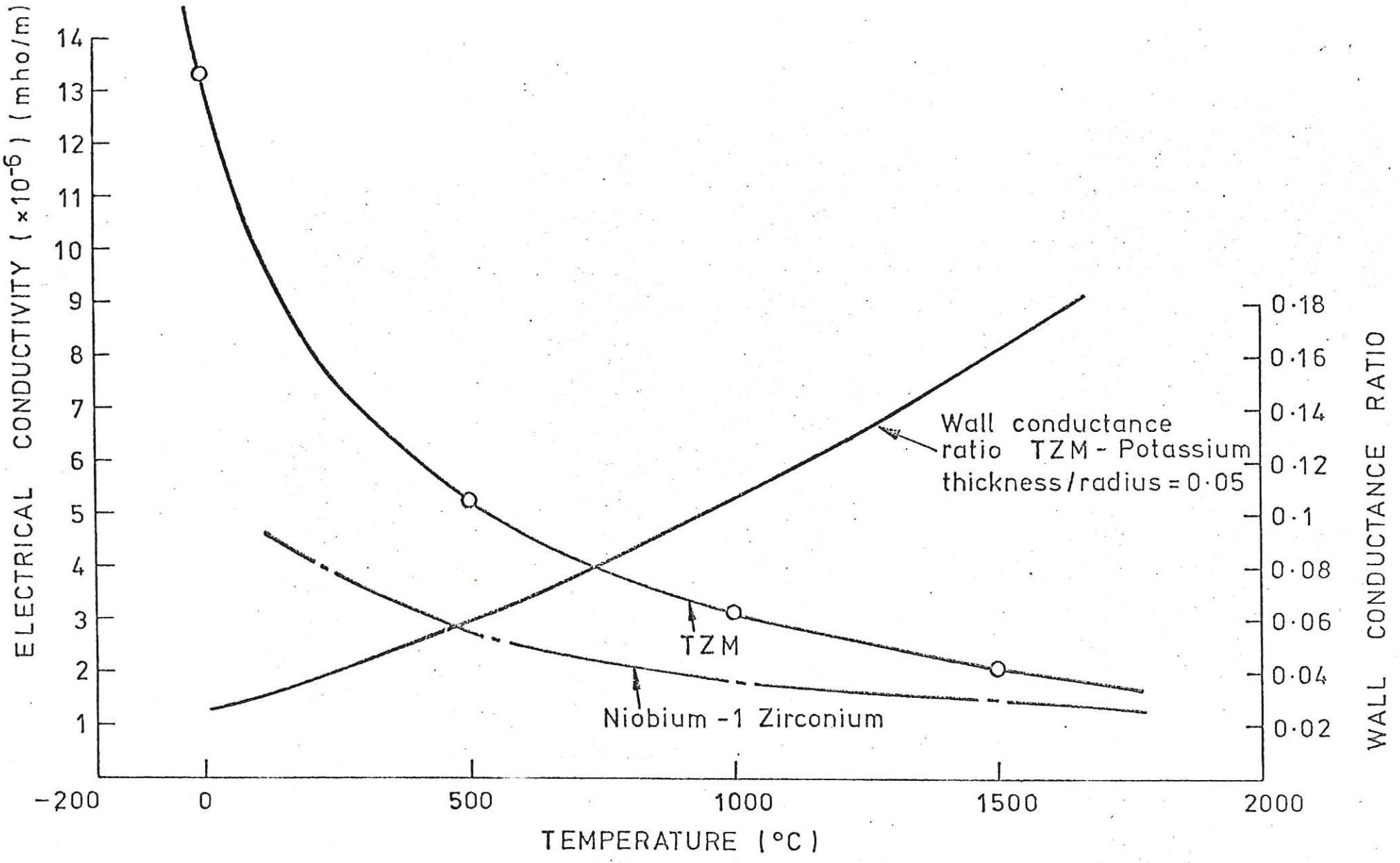

FIG. 7 ELECTRICAL CONDUCTIVITY OF TZM ALLOY AND NIOBIUM -1 ZIRCONIUM

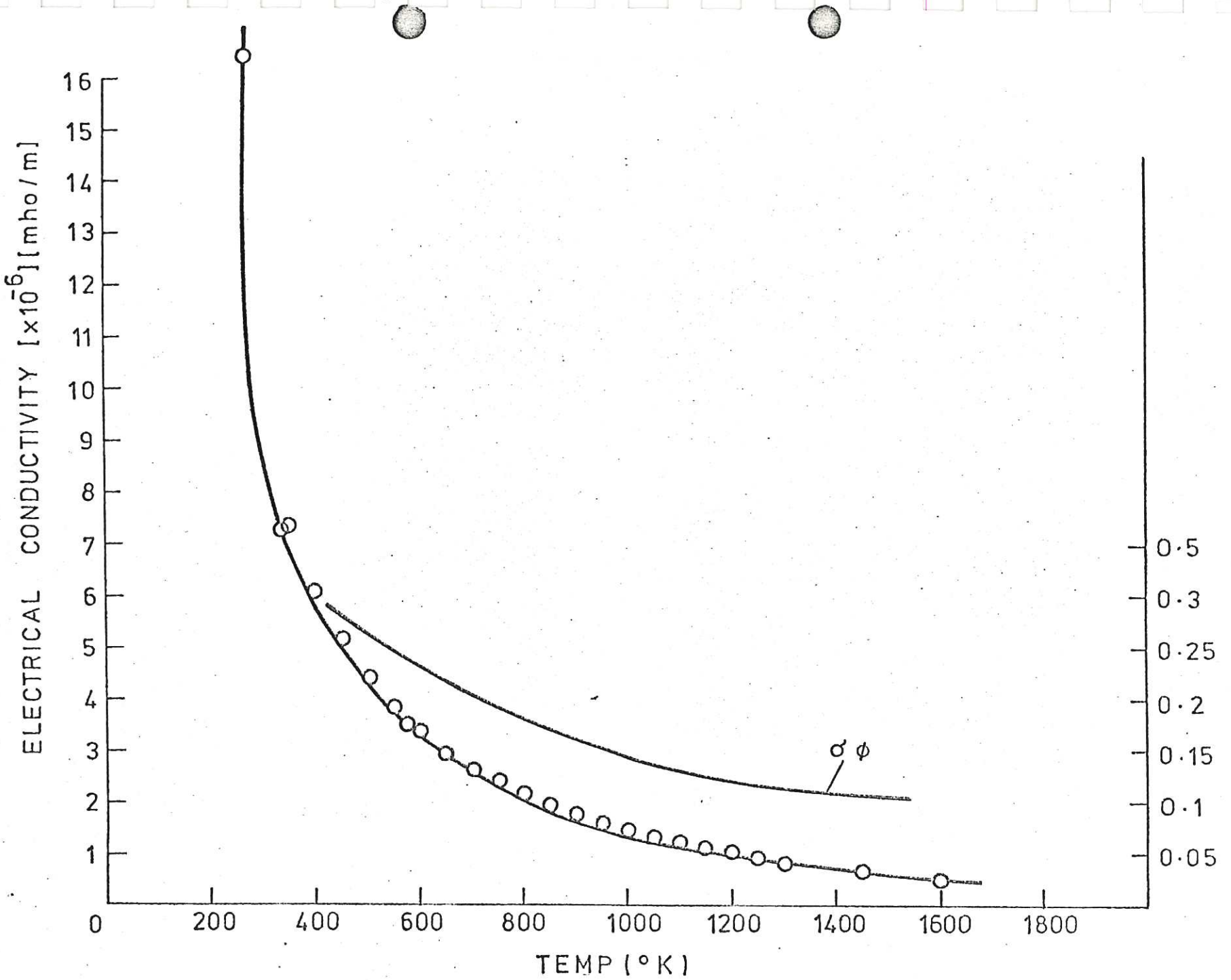

FIG. 8 ELECTRICAL CONDUCTIVITY OF POTASSIUM

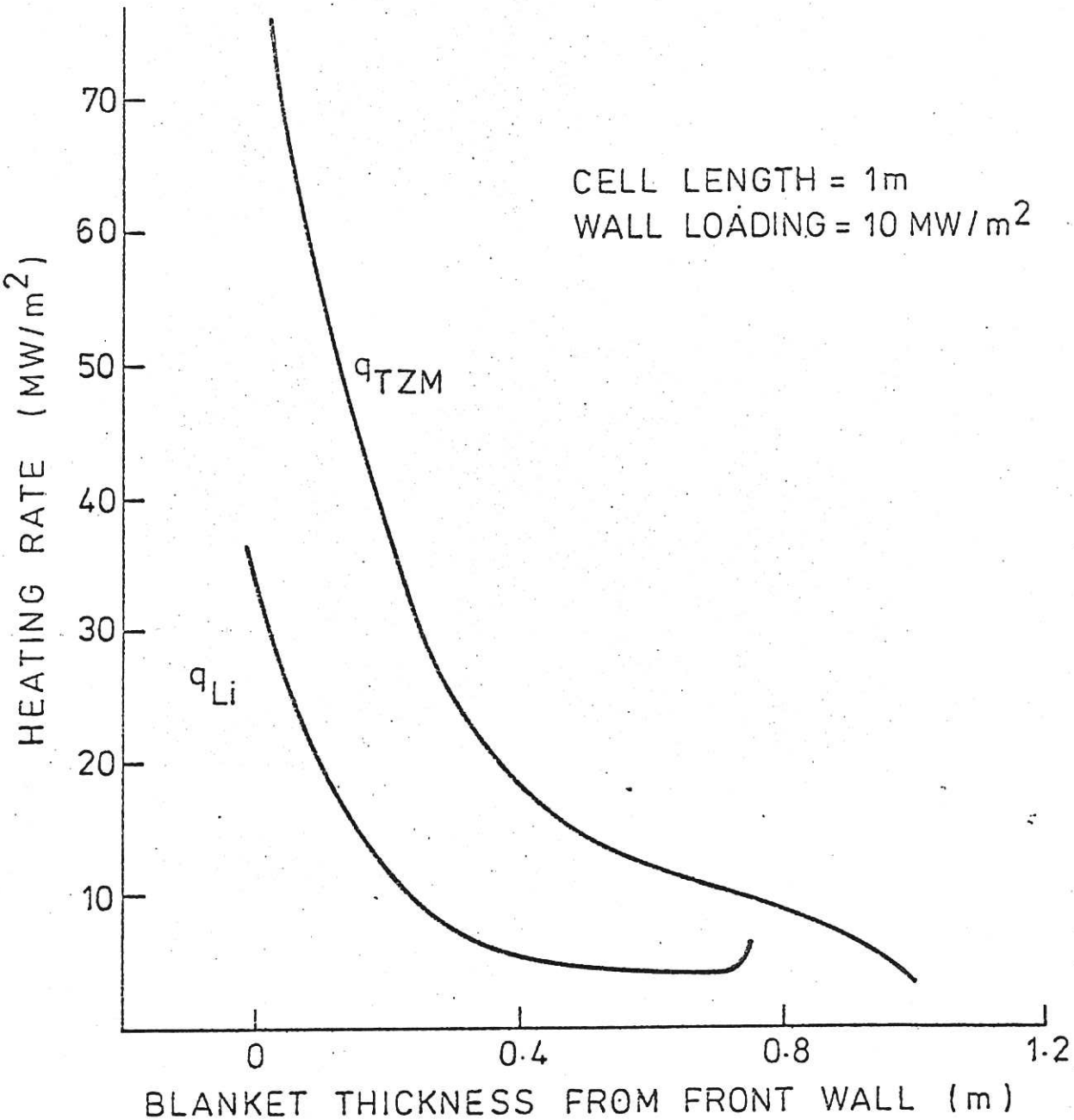

FIG. 9. A COMPARISON OF HEATING RATES IN THE TZM STRUCTURE AND LITHIUM OF A FUSION REACTOR BREEDING BLANKET.

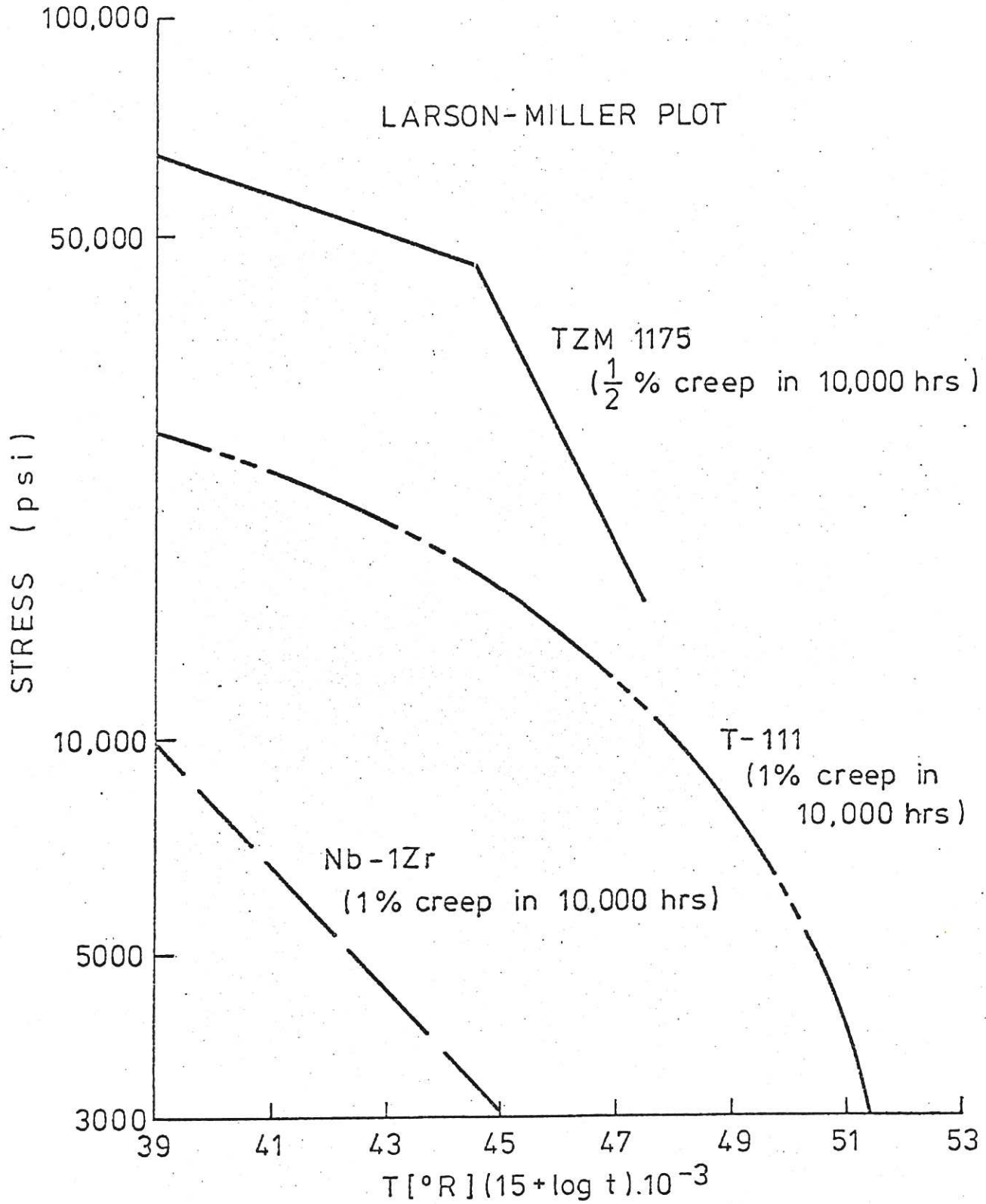

FIG. 10. STRESS VARIATION WITH TEMPERATURE AND TIME FOR SPECIFIED CREEP RATES IN TZM, Nb-1Zr AND T-111

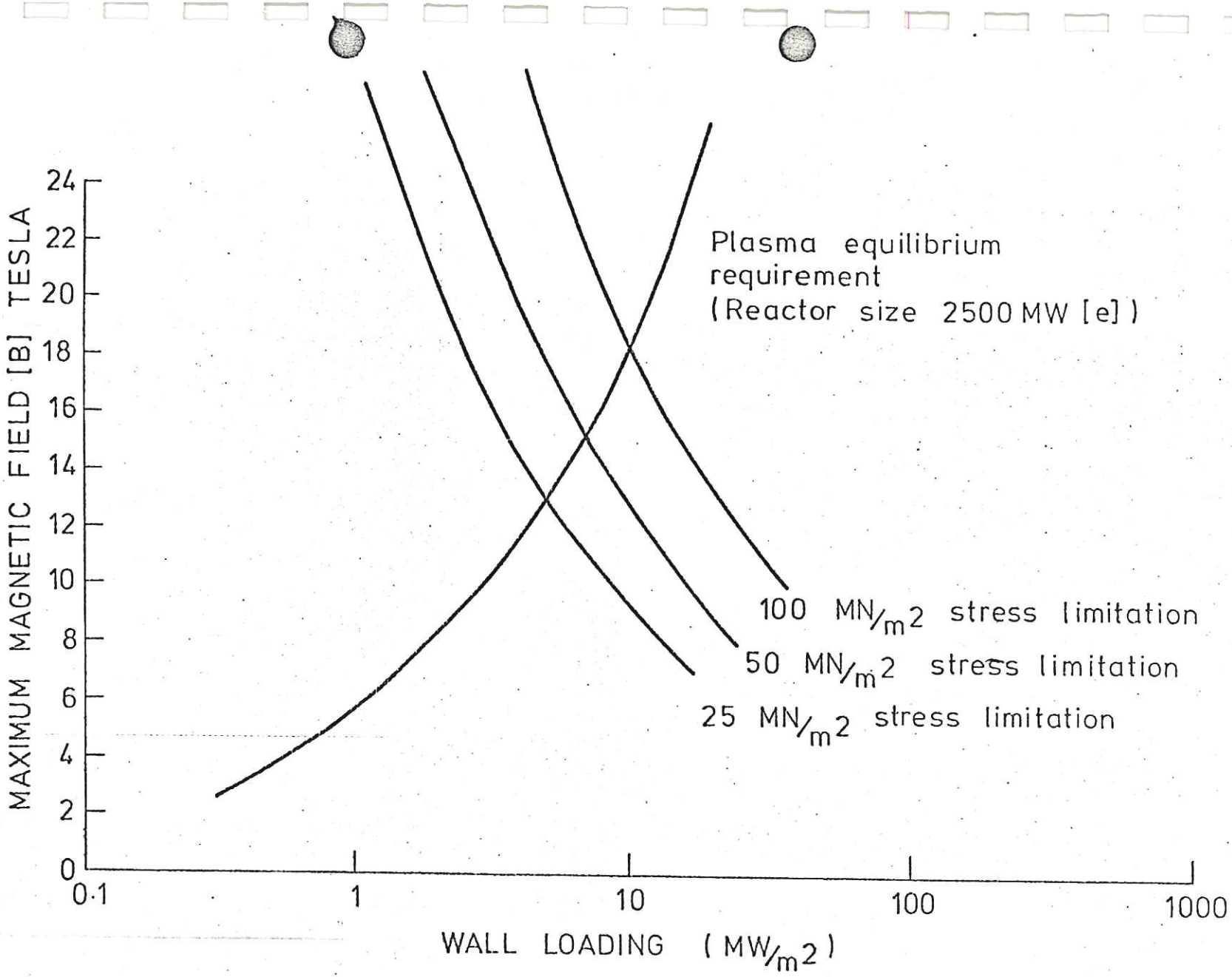

FIG.11. LIMITATIONS ON REACTOR FIRST WALL LOADING IMPOSED BY STRESSING OF A SODIUM COOLED BLANKET. CURVES FOR MAXIMUM STRESS LEVELS OF 100, 50, 25 MN/m^2 ARE SHOWN

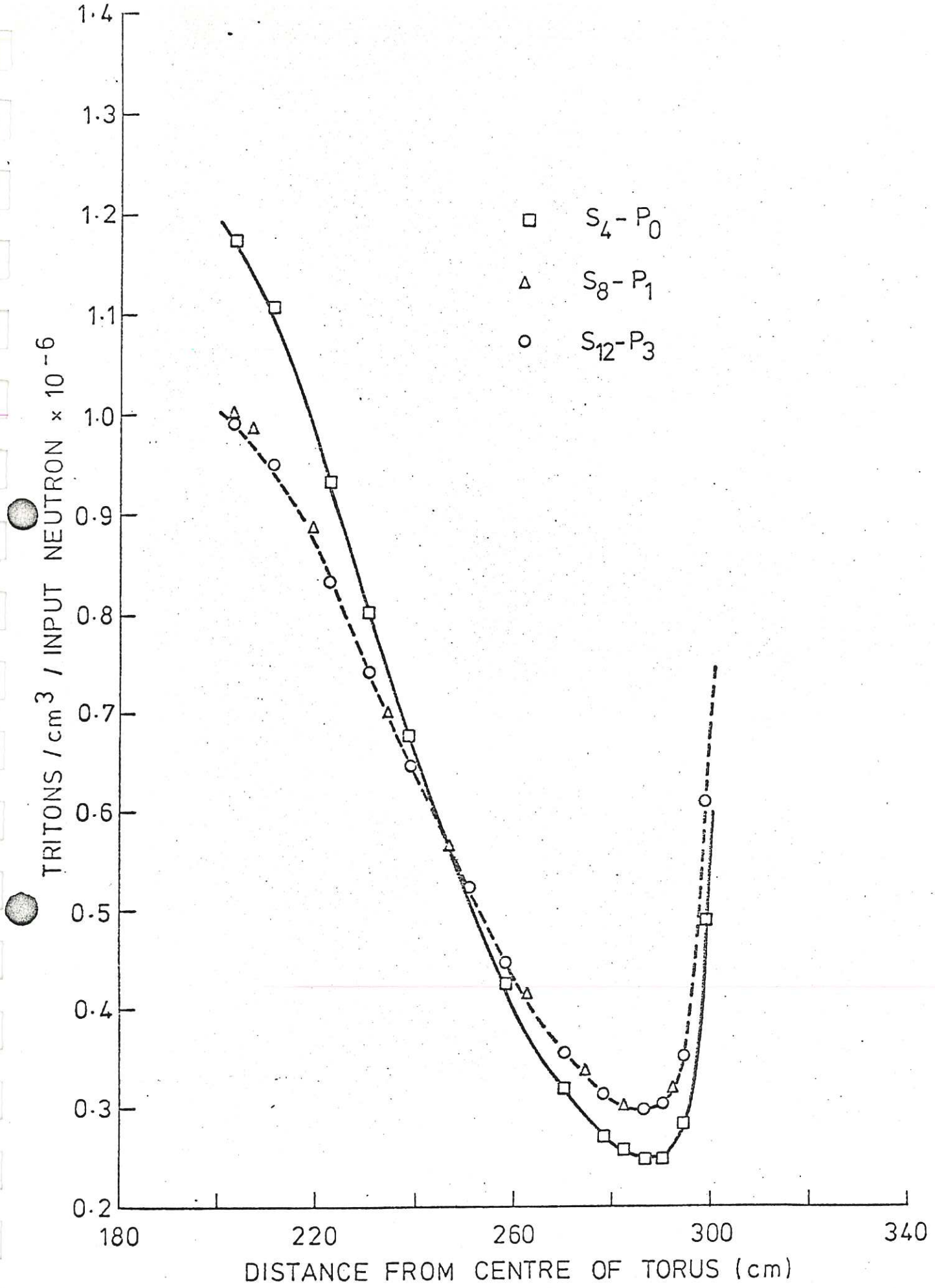

FIGURE .12. THE DISTRIBUTION OF $^{6}Li(n, \alpha)t$ REACTIONS FOR VARIOUS NEUTRON TRANSPORT APPROXIMATIONS.

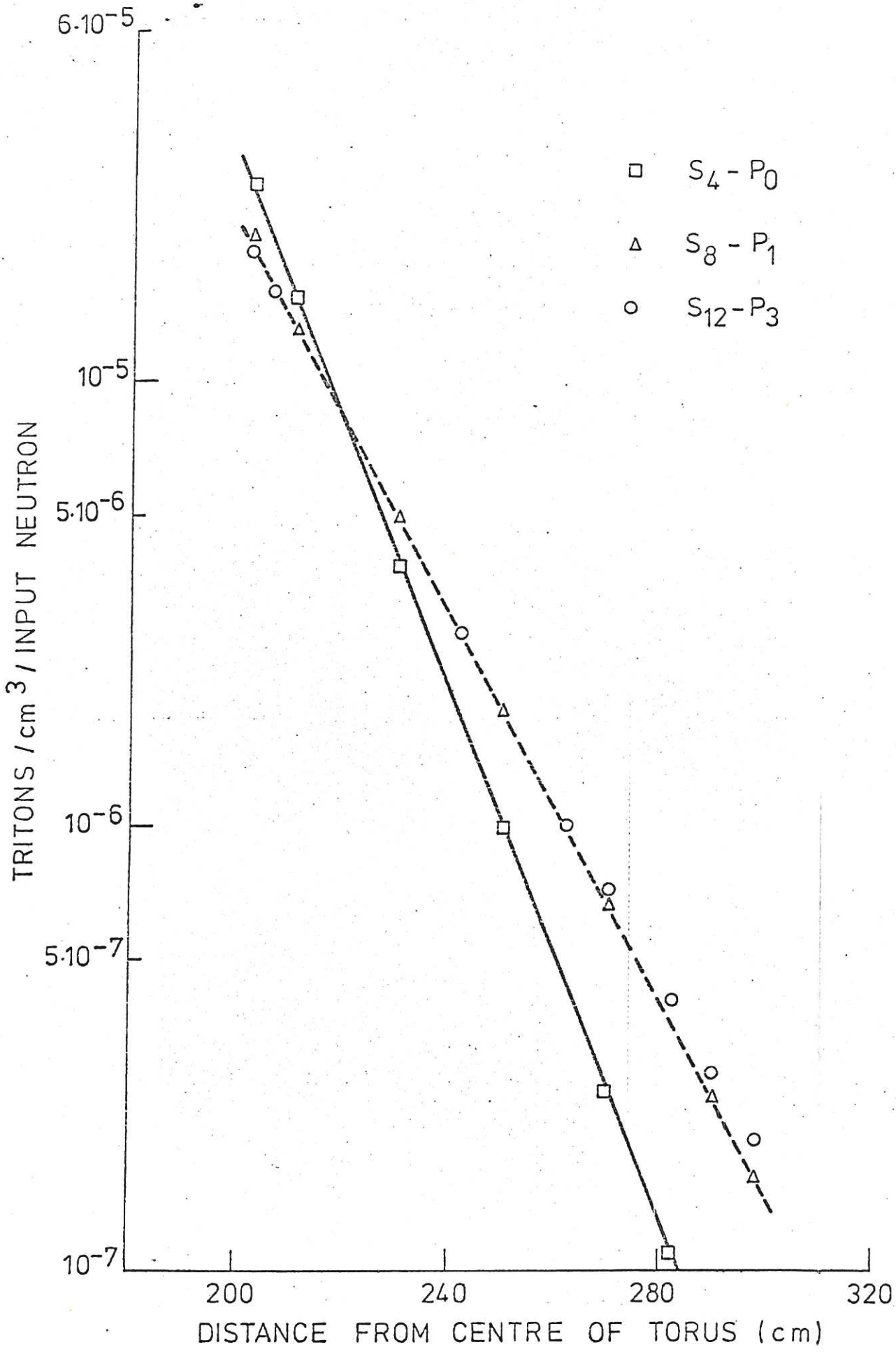

FIG. 13. THE DISTRIBUTION OF $^{7}Li(n,n'\alpha)t$ REACTIONS FOR VARIOUS NEUTRON TRANSPORT APPROXIMATIONS.

Appendix A Basic Relationships

In computing the pressure drop in component of the primary circuit, the following assumptions are made:

1) All liquid flows inside the magnet winding are laminar because of MHD effects.

2) The magnetic field within the magnet winding has the distribution given below:

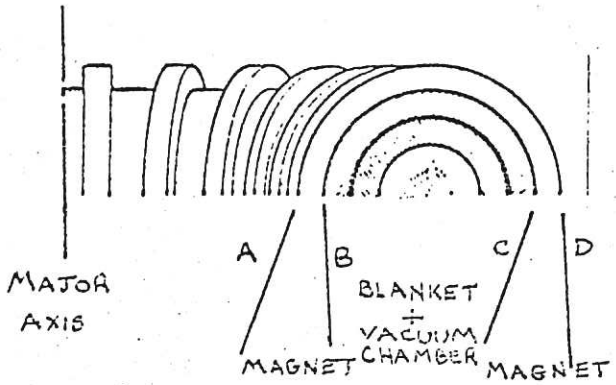

Figure A.1.

At point X between A and B at a distance x from A:

$$B_x = B_{max} \frac{x}{R_B - R_A} \quad \text{.... A-1}$$

where R_A, R_B are the radii of points A, B respectively from the major axis of the torus.

At point Y between B and C, distance y from B:

$$B_y = B_{max} \cdot \frac{R_B}{R_y} \quad \text{.... A-2}$$

At point Z between C and D, distance z from C:

$$B_Z = B_{max} \left\{ \frac{R_D - R_C - z}{R_D - R_C} \right\} \quad \text{.... A-3}$$

It is assumed that the field strength varies linearly from B_{max} to $B_{max} \cdot \frac{R_B}{R_C}$ at the inner magent surface.

Potassium flowrates:

Let a standard cell have a length 1 metre, depth 1 metre and a width of 0.3 metres. Heat release/cell is then $0.3P_W$ watts. Potassium flowrate per cell is then given by:

$$\dot{M} \ (C_p \Delta T_{subi} + \lambda) = 0.3P_W \quad \text{.... A-4}$$

where $\dot{M}$ is the mass flowrate of potassium/cell

C_p is the liquid potassium specific heat,

ΔT_{subi} is the inlet subcooling,

and λ is the latent heat heat of potassium.

A subcooling of 300°C may be shown to be sufficient to ensure liquid only flow to the front wall. Then:

$$\dot{M} = 0.143 \cdot 10^{-6} P_W \quad \text{.... A-5}$$

For ducts carrying single-phase liquid potassium:

$$V_L = 0.276 \cdot 10^{-9} P_W/D^2 \quad \text{.... A-6}$$

For ducts carrying single-phase potassium vapour at near atmospheric pressure:

$$V_V = 0.34 \cdot 10^{-6} P_W/D^2 \quad \text{.... A-7}$$

Appendix B

Primary cooling circuit pressure drop calculations

The primary cooling circuit for a potassium cooled fusion reactor blanket is shown in figure B-1.

The pressure variation around the primary circuit is computed by assuming that a static head of 1 bar exists at the pump inlet. The absolute pressure at the pump inlet is thus 2 atmospheres and the pump is sized to give the total required flowrate at the pressure drop computed from primary circuit considerations. Each component in the primary circuit is taken in turn and its pressure drop is computed.

1. Pump-reactor supply line:-

In this line, flow and potassium is entirely liquid, the temperature is approximately 550°C and the pressure drop is entirely frictional. Let a single line supply one hundred cells and let the diameter of this supply line be 30 centimetres, then the Reynolds number of flow is given by;

$$Re = \frac{\rho_L V_L D}{\mu_L} = 0.095 . 10^{-2} . P_w / D \qquad \ldots\ldots B\text{-}1$$

$$\Delta P = 1.2 \left\{ \frac{4 f L}{D} \cdot \frac{\rho_L V_L^2}{2} \right\} \qquad \ldots\ldots B\text{-}2$$

The length of the duct is equal to the major toroidal radius.

A factor of twenty percent is added to the frictional pressure drop to allow for the effect of bends.

Pressure drops in the pump-reactor supply line are computed at wall loadings of 1, 5 and 10 MW/m^2 and these results are given in Table B-1o.

2. Inlet duct through magnet and magnet shield:-

Assume that a constant area fraction of the inner magnet surface is available for the passage of ducts. Mitchell and George[5] suggest that 0.1 is a reasonable value for this fraction.

The inner magnet surface area $= 4\pi^2 R. \; r_{mi}$;

where R is the major radius of the toroid and

r_{mi} is the minor radius to the inner magnet surface.

Hence total area available for the passage of ducts through the magnet and magnet shield is $0.4\pi^2 R r_{mi}$.

The number of cells in the reactor is given by; $\dfrac{4\pi^2 R r_{minor}}{0.3}$

Hence total duct area (inlet and outlet) per cell = $\dfrac{0.03\, r_{mi}}{r_{minor}}$

Total duct area/cell is given as a function of reactor loading in the table below for a 2500 MW(e) reactor;

P_w (MW/m^2)	1	5	10
total duct area/cell (m^2)	0.0384	0.0488	0.0567
total no. of cells	26000	5240	2600

TABLE B-1 Total duct area per blanket cell

It is desirable to split the total area available for passing ducts into areas for the inlet ducts and areas for outlet ducts in such a proportion that the overall pressure drop is minimised. The procedure for determining inlet and outlet duct sizes is given in Appendix F. It is found that inlet ducts require larger areas than exit ducts, the size of the exit duct being determined by limits set on the mach number of the potassium vapour. If compressibility effects are taken into account, the following duct sizes/cell are found;

wall loading (MW/m^2)	1	5	10
Maximum magnetic field intensity (tesla)	7	14	19
ratio inlet/outlet duct areas	9.08	2.44	1.0
exit duct vapour velocity (m/s)	30.8	94.3	94.3

Table B-2 Optimised Duct areas per blanket cell

Pressure Drop in the Magnet Region of the inlet duct

The MHD pressure drop in the magnet region is given by;

$$\Delta P = 1.2\, u_L \sigma_e \phi \int B^2 dl \qquad \text{.....B-3}$$

A factor of 20% has been allowed to account for the effect of bends. The integral in the above equation has been evaluated by assuming that the magnetic field intensity rises linearly from zero to B_{max} over the winding thickness. Equation B-3 is based on the assumption that flow is laminar.

As 100 cells are supplied by a single inlet duct mean liquid velocity is

$$14.3 \quad 10^{-6} \; P_w / \frac{\pi}{4} D^2 \rho_L \quad \text{then equation B-3 becomes;}$$

$$\Delta p = 0.1 \; .10^{+6} \; u_L \; B^2_{max} / D^2 \qquad \text{.....B-4}$$

where the wall conductance ratio has been assumed to be 0.185 (at a temperature of approximately 750°K).

Hence the liquid velocity in the inlet duct is given below in table B-3;

P_w ($MW/_m2$)	1	5	10
area of outlet duct (m^2)	0.381	1.42	2.84
area of inlet duct (m^2)	3.46	3.45	2.84
liquid velocity in inlet duct (m/s)	0.59×10^{-2}	0.22×10^{-1}	0.72×10^{-1}
pressure drop (N/m^2)	2.89×10^{4}	0.432×10^{6}	2.6×10^{6}

where
single
duct
supplie
100 cel

Table B-3 Liquid potassium velocity in inlet duct

Pressure drop in the magnet shield; (inlet duct)

The MHD pressure drop in the inlet duct in traversing the magnet shield;

$$\Delta p = 1.2\, u_L \sigma_e \phi \int_0^{0.8} \left(B_{max} \frac{R_B}{R_y}\right)^2 dy \qquad \text{.....B5}$$

where R_B and R_y are defined in Appendix A. for wall loadings of 1,5 and 10 MW/m^2 the shield pressure drop is given below;

P_w wall loading (MW/m^2)	1	5	10
$\left\{\frac{R_B^2}{R_B + y}\right\}_{0.8}^{0}$ (m)	0.78	0.72	0.71
Δp (N/m^2)	0.049×10^6	0.93×10^6	5.6×10^6

Table B-4 Pressure drop in the inlet duct in traversing the magnet shield

Frictional pressure drop in the inlet ducts may be shown to be negligible compared with the magnetohydynamic pressure loss, and has consequently been neglected.

Pressure loss in the inlet manifold of the blanket cell:-

Assume that the flow is normal to the magnetic field within the superconducting windings and has a cross-sectional area given in the table below. The M.H.D. pressure drop incurred by flow radially towards the minor axis of the torus is thus;

$$\Delta p_R = 1.2\, u_R \sigma_e \phi B_{max}^2 \left\{\frac{R_B}{R_B + y}\right\}_{0.8}^{1.8} \qquad \text{.....B6}$$

$P_w (MW/m^2)$	1	5	10
area of inlet duct (m^2)	0.0346	0.0346	0.0284
area of outlet duct (m^2)	0.0038	0.0142	0.0284

Table B-5 Inlet and outlet manifold cross-sectional areas of a blanket cel

In equation B-6, U_R is the liquid potassium velocity radially towards the minor axis of the torus, σ_e is the electrical conductivity of liquid potassium evaluated at 1000°K and ϕ is the wall conductance ratio at 1000°K (0.135) (based on data for TZM alloy). A twenty percent increase in pressure drop is allowed to account for the effects of bends.

Values of ΔP_R for wall loadings of 1,5 and 10 MW/m^2 are given below. Within the inlet manifold, however, the flow is not simply radial but also possesses a circumferential component which results from the flow distributing itself over the full inlet manifold from the circular inlet ducts. A conservative estimate of the pressure drop incurred by this circumferential flow is given by;

$P_w (MW/m^2)$	1	5	10
$\Delta P_R (N/m^2)$	0.0384×10^6	0.73×10^6	2.89×10^6
$\Delta P_C (N/m^2)$	0.00144×10^6	0.025×10^6	0.084×10^6

Table B-6 Pressure losses in the inlet manifold to a blanket cell

$$\Delta P_c = 1.2\, u_c\, \sigma_e\, \phi \quad 0.3 \quad \frac{R_B^2}{R^2\big|_{\frac{1}{2}\,cell}} \quad B_{max}^2 \qquad \text{.....B7}$$

where $R\big|_{\frac{1}{2}\,cell}$ is the major radius of the torus at a location midway along the cell, and u_c is the circumferential velocity component.

Values for ΔP_C at specific wall loadings of 1,5 and 10 MW/m^2 are given in the accompanying table and are observed to be small in comparison with ΔP_R.

Pressure drop in outlet manifold

Assume that flow is totally vapour in the outlet manifold. Vapour velocity is then given by;

$$V_v = \frac{\dot{m}_c}{\rho_v A_{om}} \qquad \text{.....B8}$$

where $\dot{m}_c$ is the potassium mass flow/cell

ρ_v is the density of potassium vapour

A_{om} is the cross-sectional area of the outlet manifold

The Reynolds number of the outlet vapour flow is given by;

$$Re = \frac{\rho_v V_v D}{\mu_v}$$

where D is the equivalent diameter of the outlet manifold.

The pressure drop in the outlet manifold is mainly frictional and is given by

$$\Delta P_{om} = 1.2 \left\{ \frac{4 f L}{D} \frac{\rho_v V_v^2}{2} \right\} \qquad \text{.....B9}$$

where f is the friction factor evaluated at the above Reynolds number and a 20% allowance is made to account for the effects of pipe bends.

The table below gives the frictional pressure drop as a function of wall loading;

Table B-7 Pressure drop in the outlet manifold of a blanket cell

P_w (MW/m^2)	1	5	10
Re	1×10^5	2.6×10^5	3.73×10^5
A_{om} (m^2)	0.00381	0.0142	0.0284
f	0.017	0.015	0.014
P_{om} (N/m^2)	800.0	664.0	450.0

Pressure drop in outlet duct through magnet and shield;

Assume flow is totally vapour. The pressure drop is purely frictional and is calculated in a similar manner to that for the outlet manifold. The table below gives values of the frictional pressure drop for reactor wall loadings of 1,5 and 10 MW/m^2. It is assumed that a single outlet duct services 100 cells.

Table B-8 Pressure drop in outlet duct within the reactor

P_w (MW/m^2)	1	5	10
Reynolds number	10^6	2.6×10^6	3.73×10^6
friction factor	0.012	0.010	0.0095
pressure drop (N/m^2)	100.0	81.5	55
duct diameter (m)	0.7	1.35	1.90

Pressure drop in ducts to the external heat exchangers:-

Assume that the length of the ducts is equal to the major toroidal radius for each value of reactor wall loading.

Table B-9 Pressure drop in ducting from reactor to main heat exchanger.

Wall loading (MW/m^2)	1	5	10
major radius of torus (m)	31	13.9	9.8
duct diameter (m)	0.7	1.35	1.90
$P_{E.D.}$ (N/m^2) frictional pressure drop in external ducts	1660	630	302

Pressure drop in external heat exchangers:

If it is assumed that condensation of potassium vapour occurs in the shellside of a shell and tube heat exchanger, the shellside pressure drop is given by:

$$\Delta P_s = \frac{FG^2 D_s (N+1)}{5.22 \cdot 10^{10} \cdot D_e S \cdot \phi_s} \qquad \text{.....B.10}$$

where f is a dimensionless friction factor

G is the mass velocity

D is the tube diameter

N is the number of shellside baffles

D_e is the equivalent diameter for heat transfer and pressure drop

S is the specific gravity

ϕ_s is the viscosity ratio $(\mu/\mu \text{ water})^{0.14}$ for shellside

If twenty tubes are assumed in a square pitch arrangement;

D_e = 4 x free area/wetted perimeter.

$$Re_s = \frac{D_e G_s}{\mu} \quad ; \quad \text{for} \quad d_s \sim 0.5m, \quad f \sim 0.00175, \quad Re_s \sim 25{,}000$$

$$\Delta P_s = 0.1 \cdot 10^5 \ N/m^2$$

It is assumed that the pump is situated close to the condenser outlet and that pressure drop between the pump and condenser is small.

A summary of component pressure losses in the primary coolant circuit is given in the following table:-

Table B-10 Summary of primary circuit pressure losses

Primary circuit component	Pressure Drop(MN/m^2) for wall loadings of 1 MW/m^2	5 MW/m^2	10 MW/m^2
pump-reactor supply line	2.19×10^{-4}	2.06×10^{-3}	4.75×10^{-3}
inlet duct through magnet and magnet shield	0.078	1.36	8.2
inlet manifold pressure drop	0.0398	0.755	2.99
wicked configuration (in 2 phase region)	1×10^{-3}	1×10^{-3}	1×10^{-3}
once through evaporator configuration (in 2 phase region)	1.26×10^{-3}	3.1×10^{-2}	1.26×10^{-1}
outlet manifold	8×10^{-4}	6.6×10^{-4}	4.5×10^{-4}
outlet duct through magnet and shield	1×10^{-4}	8×10^{-5}	5.5×10^{-5}
pressure drop in ducts to external heat exchangers	1.66×10^{-3}	6.3×10^{-4}	3.02×10^{-4}
pressure drop in the external heat exchangers	0.1×10^{-1}	0.1×10^{-1}	0.1×10^{-1}
Total	0.134 MN/m^2	2.16	11.3
	(19.7 psia)	(320 psia)	(1660 psia)
Ratio of MHD pressure drop/ total pressure drop	0.89	0.98	0.99

Simplified analysis of primary circuit pressure loss:-

The preceeding analysis of primary circuit pressure distribution has shown that the pressure losses caused by MHD effects in the magnet shield, magnet and inlet manifold regions dominate the circuit. If other resistances in the circuit are ignored then the total pressure drop in the primary circuit may be approximated by the equation:

$$\Delta_{P.C.} = \overbrace{1.2\, u_D (\sigma\phi)_D \left\{ \int_0^1 B_{max}^2 \left(\frac{x}{R_B - R_A} \right)^2 dx \right\}}^{\text{MAGNET}}$$

$$+ \overbrace{1.2\, u_D (\sigma\phi)_D \left\{ \int_0^{0.8} B_{max}^2 \left(\frac{R_B}{R_y} \right)^2 dy \right\}}^{\text{MAGNET SHIELD}}$$

$$+ \overbrace{1.2\, u_c (\sigma\phi)_c \left\{ \int_{0.8}^{1.8} B_{max}^2 \left(\frac{R_B}{R_y} \right)^2 dy \right\}}^{\text{INLET MANIFOLD}} \qquad \text{..... B-7}$$

where $\Delta P_{P.C.}$ is the total pressure drop in the primary coolant circuit.

However;

$$\left.\begin{aligned} \int_0^1 B_{max}^2 \left(\frac{x}{R_B - R_A} \right)^2 dx &= 0.33\, B_{max}^2 \\ \int_0^{0.8} B_{max}^2 \left(\frac{R_B}{R_y} \right)^2 dy &= 0.75\, B_{max}^2 \\ \int_{0.8}^{1.8} B_{max}^2 \left(\frac{R_B}{R_y} \right)^2 dy &= 0.8\, B_{max}^2 \end{aligned}\right\} \text{ for wall loadings from 1-10 MW/m}^2$$

The factors 0.75 and 0.8 in the evaluation of the above integrals are strictly not constant but are weak functions of wall loading. The figures 0.75 and 0.8 are mean values and the maximum error incurred by their use is 5%, for wall loadings between and 1 and 10 MW/m^2. Hence;

$$\Delta P_{P.C.} = B_{max}^2 \left[1.3\, u_D (\sigma\phi)_D + 0.96\, u_c (\sigma\phi)_c \right]$$

..... B-8

For ducting through the magnet and magnet shield the mean temperature is approximately 550°C hence $(\sigma\phi)_D = 0.2$ (from figure 8) - in the cell inlet manifold the mean temperature = 800°C and hence $(\sigma\phi)_C = 0.135$

$$\text{Now } U_D = 0.006\, P_W \cdot 10^{-6}$$

$$U_C = 0.0064\, P_W \cdot 10^{-6}$$

Hence, $\Delta P_{P.C.} = 0.024\, P_W\, B_{max}^2 \cdot 10^{-6}$ ... B-9

However, the maximum hoop stress f_{max} in the ducts is given by;

$$f_{max} = \frac{\Delta P_{P.C.}}{0.05}$$ when the duct wall thickness to radius ratio is 0.05. Inserting equation B-9 yields

$$f_{max} = 0.048 \cdot \frac{P_W}{10^6} \cdot B_{max} \quad \text{... B-10}$$

This relationship is shown graphically in figure 6 and with the limitations imposed by plasma equilibrium considerations the reactor wall loading limitations can be read as a function of the maximum permissible stress in the duct wall.

This analysis has:

(1) allowed for the distribution of flow around the toroidal minor axis within each cell. No allowance has been made, however, for bulk flow of coolant around the minor axis. This implies that all cells which receive coolant from a single inlet duct are situated at the same circumferential position as the minor axis. Inclusion of circumferential flow around the minor axis to account for distribution of potassium to cells at varying circumferential locations would increase the primary circuit pressure drop by approximately 30%.

(2) shown that the frictional pressure drops in the primary coolant circuit are only about 10% of the total pressure loss at a wall loading of 1 MW/m^2 and about 1% at a wall loading of 10 MW/m^2.

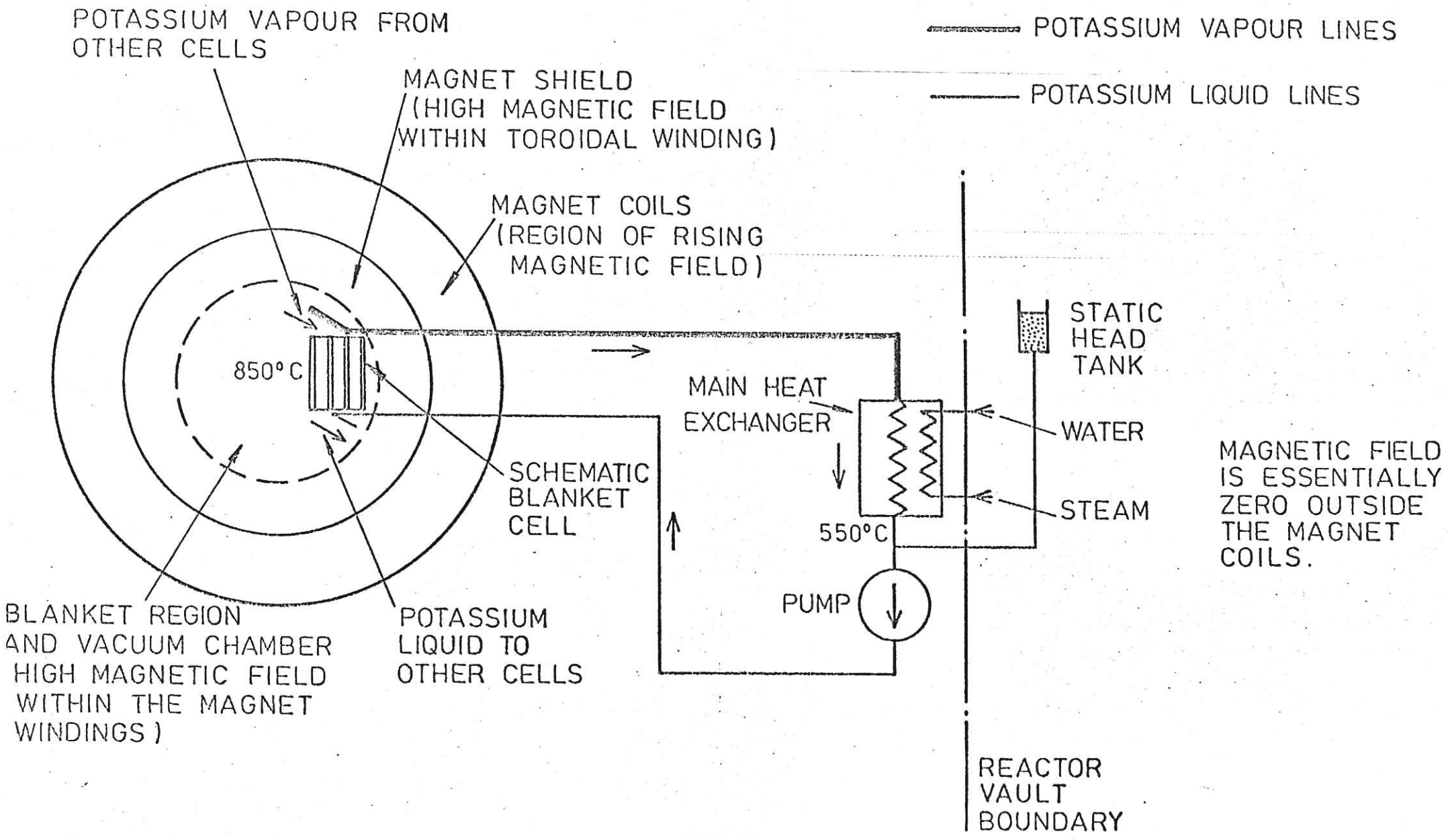

FIG. B-1 THE PRIMARY COOLING CIRCUIT.

APPENDIX C

MODEL OF CONVECTIVE BOILING IN A POROUS WICK

In this appendix a model is presented of convective boiling of a conducting fluid in a porous wick. It is based on the model of Macbeth[25] but is extended to include the effects of magnetohydrodynamic forces on the liquid phase.

For wick covered surfaces, the fluid driving force within the wick is capillary pumping power. The potassium has to be vaporised within the capillary structure; this is necessary to ensure the interface between the phases is within the porous medium. At an evaporating surface, evaporation causes the radius of curvature at the meniscus to increase while at the potassium inlet, the radius of curvature remains constant. This difference in radius of curvature provides the capillary force. The pressure difference created is;

$$\Delta p = 4\sigma \left\{ \frac{\cos \alpha_e}{D_e} - \frac{\cos \alpha_i}{D_i} \right\} \qquad \ldots \text{C.1.}$$

where σ is the surface tension (N/m)

D_e is the diameter of capillary pores in the evaporation zone (m)

D_i is the diameter of capillary pores at liquid inlet (m)

α_e is the contact angle in the evaporated zone (−)

α_i is the contact angle at liquid inlet (−)

This pressure difference is available to overcome resistance to circulation due to friction, changes of momentum, gravity and MHD pressure loss. The static pressure difference across the wick may be expressed;

$$\Delta P_c = \{ P_2 - P_1 \} + \{ \Delta P_F + \Delta P_{MHD} + \Delta P_{MOM} \} \qquad \ldots \text{C-2}$$

where ΔP_C is the capillary driving force (N/m^2)

ΔP_F is the frictional pressure drop (N/m^2)

ΔP_{MHD} is the magnetohydrodynamic pressure drop (N/m^2)

ΔP_{MOM} is the static pressure drop caused by momentum changes (usually small) (N/m^2)

$(P_2 - P_1)$ is the overall pressure drop across the wick (N/m^2)

The frictional pressure drop is evaluated on the assumption that the flow is laminar within the pores so that;

$$\Delta P_{L,V} = 32\,h \left\{ \frac{\mu V}{D^2} \right\}_{L,V} \quad \ldots C\text{-}3$$

where h is the wick thickness (m)

μ is the absolute viscosity (kg/ms)

V is the fluid velocity (m/s)

and D is the characteristic pore size of the wick (m)

subscripts, L, V denote liquid and vapour respectively.

The pressure drop due to momentum changes is simply

$$\Delta P_{MOM} = \left[\rho V^2 \right]_{L,V} \quad \ldots C\text{-}4$$

where ρ is the fluid density

The magnetohydrodynamic pressure drop is only applicable to the liquid filled pores of the wick which are envisaged as small circular ducts. A conservative estimate of the MHD pressure drop is :-

$$\Delta P_{M.H.D} = \sigma_e B^2 V_L h \quad \ldots C\text{-}5$$

where B is the applied transverse magnetic field (tesla) and σ_e is the electrical conductivity of the liquid phase (mho/m).

The basic assumption is now made that liquid is fed by capillary action from the body of the wick to the hot surface where evaporation occurs. The larger volumetric flowrate of the vapour tends to force it into the larger pores. Thus, for liquid flow ;

$$\frac{4\sigma}{D_L} = \left\{ P_2 - P_1 \right\} + 32\,h \left\{ \frac{\mu V}{D^2} \right\}_L + \sigma_e B^2 V_L h \quad \ldots C\text{-}6$$

where (P_2-P_1) is the overall pressure drop across the wick and D_L is a characteristic size of liquid pores.

For vapour flow;

$$\left\{ P_2 - P_1 \right\} = \frac{4\sigma}{D_V} + 32\,h \left\{ \frac{\mu V}{D^2} \right\}_V + \left\{ \rho V^2 \right\}_V \quad \ldots C\text{-}7$$

where D_V is the characteristic size of the vapour pores. Hence eliminating (P_2-P_1);

$$4\sigma \left\{ \frac{1}{D_L} - \frac{1}{D_V} \right\} = 32\,h \left\{ \left[\frac{\mu V}{D^2} \right]_L + \left[\frac{\mu V}{D^2} \right]_V \right\} + \left[\rho V^2 \right]_L + \left[\rho V^2 \right]_V + \sigma_e B^2 V_L h. \quad \ldots C\text{-}8$$

If the following quantities are introduced ;

α = effective void fraction

N = total number of holes/unit area

yN = number of holes of diameter D_V

Optimized wick parameters

magnetic field strength B (tesla)	max. heat flux Ø (MW/m^2)	wick thickness (m)	liquid capillary size D_L (m)	vapour capillary size D_V (m)	void fraction x (–)	pressure drop across wick (N/m^2)	fraction of holes for vapour flow (y)	No of holes/ unit area N
1	7.1	0.1×10^{-3}	2×10^{-3}	1×10^{-2}	0.71	0.84×10^{2}	0.2×10^{-4}	0.3×10^{7}
5	5.1	0.1×15^{-3}	5×10^{-4}	5×10^{-2}	0.71	0.45×10^{3}	0.2×10^{-4}	0.3×10^{7}
10	3.5	0.1×10^{-3}	5×10^{-4}	5×10^{-2}	0.71	0.41×10^{3}	0.2×10^{-4}	0.3×10^{7}
15	3.2	0.1×10^{-3}	5×10^{-4}	5×10^{-2}	0.71	0.34×10^{3}	0.2×10^{-4}	0.3×10^{7}
20	3.0	0.1×10^{-3}	5×10^{-4}	5×10^{-2}	0.71	0.27×10^{3}	0.2×10^{-4}	0.3×10^{7}
1	5.1	1×10^{-3}	5×10^{-3}	1×10^{-2}	0.71	0.34×10^{2}	0.2×10^{-4}	0.3×10^{7}
5	3.0	1×10^{-3}	5×10^{-4}	5×10^{-2}	0.71	0.33×10^{3}	0.2×10^{-4}	0.3×10^{7}
10	1.9	1×10^{-3}	5×10^{-4}	5×10^{-2}	0.71	0.13×10^{3}	0.2×10^{-4}	0.3×10^{7}
15	1.5	1×10^{-3}	5×10^{-4}	5×10^{-2}	0.71	0.44×10^{2}	0.2×10^{-4}	0.3×10^{7}
20	0.8	1×10^{-3}	5×10^{-4}	5×10^{-2}	0.71	0.19×10^{2}	0.2×10^{-4}	0.3×10^{7}
1	3.2	1×10^{-2}	5×10^{-4}	5×10^{-2}	0.71	0.4×10^{3}	0.2×10^{-4}	0.3×10^{7}
5	1.1	1×10^{-2}	5×10^{-4}	5×10^{-2}	0.71	0.38×10^{2}	0.2×10^{-4}	0.3×10^{7}
10	0.3	1×10^{-2}	5×10^{-2}	5×10^{-2}	0.71	0.7×10^{2}	0.2×10^{-4}	0.3×10^{7}
15	0.2	1×10^{-2}	5×10^{-4}	5×10^{-2}	0.71	0.5×10^{1}	0.2×10^{-4}	0.3×10^{7}

Optonized wick parameters (Cont.)

magnetic fields strenght B (tesla)	max. heat flux ϕ (MW/m^2)	wick thickness (m)	liquid capillary size D_v (m)	vapour capillary size D_l (m)	void fraction x (-)	pressure drop across wick (N/m^2)	fraction of holes for vapour flow (Y)	No of holes/ unit area N
20	0.1	1×10^{-2}	5×10^{-4}	5×10^{-2}	0.71	0.48×10^{1}	0.2×10^{-4}	0.3×10^{7}
1	1.9	1×10^{-1}	5×10^{-4}	5×10^{-2}	0.71	0.13×10^{3}	0.2×10^{-4}	0.3×10^{7}
5	0.1	1×10^{-1}	5×10^{-4}	5×10^{-2}	0.71	0.51×10^{1}	0.2×10^{-4}	0.3×10^{7}
10	0.025	1×10^{-2}	5×10^{-4}	5×10^{-2}	0.71	0.46×10^{2}	0.2×10^{-4}	0.3×10^{7}
15	0.01	1×10^{-1}	5×10^{-4}	0.45×10^{-1}	0.68	0.52×10^{1}	0.2×10^{-4}	0.3×10^{7}
20	0.006	1×10^{-1}	5×10^{-4}	0.45×10^{-1}	0.68	0.52×10^{1}	0.2×10^{-4}	0.3×10^{7}

Table C-1

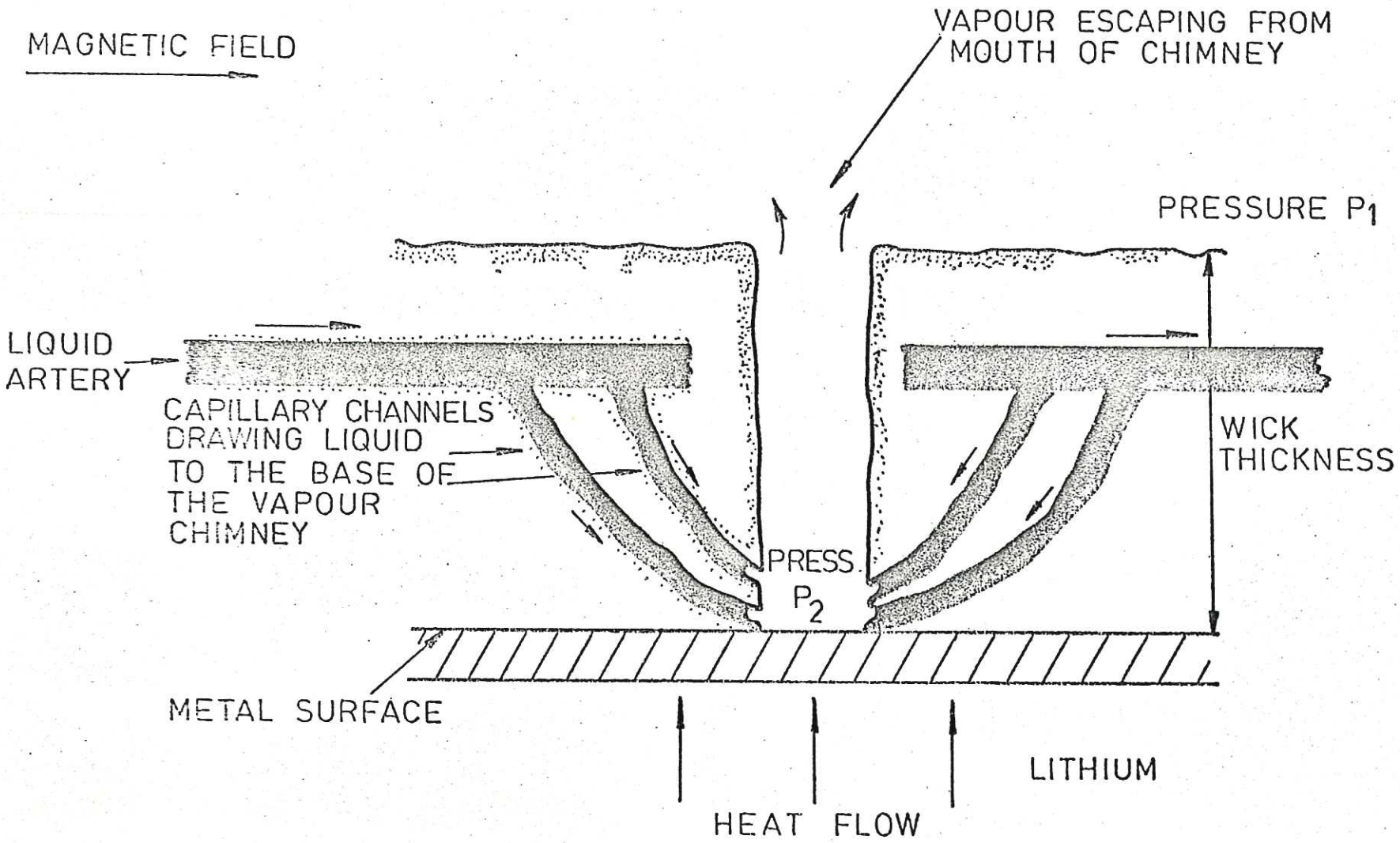

FIG. C-1 PROPOSED MODEL OF 'WICK BOILING.'

APPENDIX D

Transport Properties and Boiling Characteristics of Wicks

This appendix is a summary of current knowledge on wick systems in laminar flow in the absence of magnetohydrodynamic effects. In particular, the mechanisms which govern the maximum heat transfer rate to an overlaid surface are examined. When the various transport processes that occur during cell operation are analysed, it is found that there are two possibly interrelated phenomena which limit the maximum rate at which energy can be transferred. They are:

1. The heat flux at which apparent film-boiling occurs in the wick of the evaporator,
2. The maximum liquid flowrate that the capillary pump can provide to the evaporator.

When either of the above limiting phenomena occurs, the result is the same: any attempt to increase the net heat input to the wick produces a large temperature rise at the base of the wick. This increase of temperature is probably caused by an insufficiency of liquid at the liquid-wick-solid interface in the evaporator. The above limiting considerations are each examined and in the light of experimental data, recommendations are made concerning the preferred type of wick for application to blanket cooling of a fusion reactor by alkali liquid metal.

Limitations due to Capillary Pumping Capacity

The Laplace-Young equation of capillarity indicates that in the evaporator the difference in pressures between the liquid and vapour sides of the vapour-liquid interface

$$(P_L - P_v) = \frac{-2\sigma}{R} \qquad \ldots D\text{-}1$$

where R is the radius of curvature of the interface. For most wicking materials, $\frac{-2\sigma}{R} \approx$ 5 to 20 inches of water.

It is possible to formulate a model of the flow through a porous material. It is assumed that fluid permeates by capillary action through the wick from a feed edge and a uniform heat flux is applied at the base of the wick.

Simplified Model of a Wicked Evaporator

The following assumptions are made to make the analysis tractable:

1) The wicking material is rigid, of constant thickness 'δ' and is saturated

with a wetting liquid along the entire evaporator length 'l'. The wicking material is considered to be isotropic so that at any given cross-section of the wick, the pore area A_p and the total area of the cross-section A_t are related by:

$$\frac{A_p}{A_t} = \varepsilon ;$$

where ε is the porosity of the material.

2) The vapour and liquid are at the same constant temperature over the length of the evaporator.

3) The effects of gravity are not considered.

4) At any given point, the liquid vapour interface can be characterised by one radius of curvature R.

5) Any terms containing differentials raised to second or higher powers are neglected.

6) The heat flux is considered constant with length.

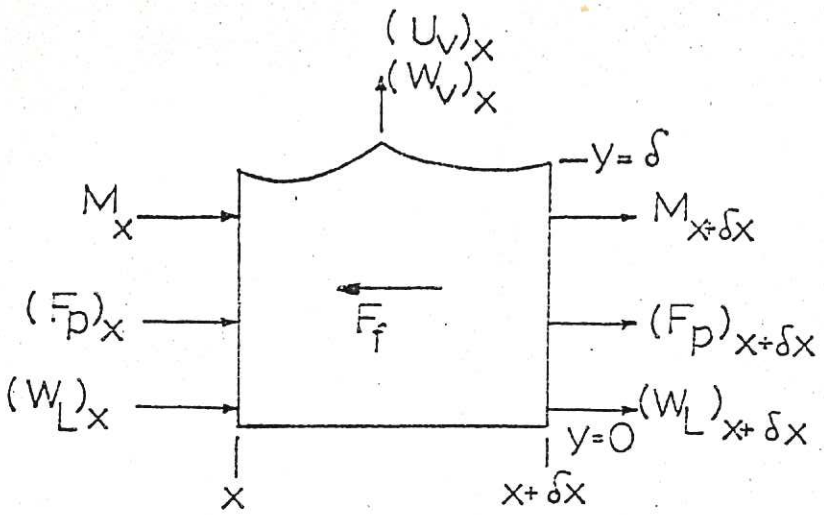

FIGURE H-1. A Differential Element of Wicking Material

Consider the differential element of wicking material shown above.

This diagram shows the forces and momentum fluxes associated with a differential element of the saturated wicking material at a given point in the evaporator.

Applying the continuity equation for the element of figure H-1 :

$$(W_L)_x - W_v = (W_L)_{x+dx} \qquad \ldots \text{D-2}$$

where W_L is the liquid mass flowrate, and W_v is vapour generation rate.

But

$$(W_L)_x = \rho_L \varepsilon \delta b \, u_L, \qquad \ldots D\text{-}3$$

where ρ_L is the liquid density, δ is the wick thickness, and b is the width of the wick, and

$$(W_L)_{x+dx} = \rho_L \varepsilon \delta b \left(u_L + \frac{du_L}{dx} dx\right) \qquad \ldots D\text{-}4$$

$$W_v = \rho_L \left(-\frac{du_L}{dx}\right) dx \varepsilon \delta b \qquad \ldots D\text{-}5$$

$$= \rho_V u_V b dx \qquad \ldots D\text{-}6$$

where ρ_V is the vapour density and u_V is the vapour velocity.

The x-momentum equation for the element is:

$$\Sigma F_x = M_{x+dx} - M_x$$

where F represents force and M, momentum

The momentum terms are $$M_x = \frac{\rho_L}{g_o} u_L^2 \varepsilon b \delta \qquad \ldots D\text{-}7$$

$$M_{x+dx} = \frac{\rho_L}{g_o} u_L^2 \varepsilon b \delta + \frac{\rho_L}{g_o} \frac{d(u_L^2)}{dx} dx \, \varepsilon b \delta \qquad \ldots D\text{-}8$$

But $$\Sigma F_x = F_p|_x - F_p|_{x+dx} - F_f \qquad \ldots D\text{-}9$$

where F_p is the pressure force and is obtained from the Laplace-Young equation.

$$F_p|_x = (P_v - \frac{2\sigma}{R}) \varepsilon \delta b; \qquad \ldots D\text{-}10$$

where σ is the surface tension and P_v is the pressure in the vapour phase.

$$F_p|_{x+dx} = \left(P_v - \frac{2\sigma}{R+dR}\right) \varepsilon \delta b \qquad \ldots D\text{-}11$$

$$F_p\big|_x - F_p\big|_{x+dx} = -\varepsilon\delta b 2\sigma \frac{dR}{R^2} \qquad \text{... D-12}$$

Because of the low flow rates and velocities encountered with capillary flow in the wicks, the flow produced by the net capillary force can be assumed to be both laminar and relatively free from inertia effects. Both of these conditions must be met if Darcy's law for flow through porous media is to apply. Darcy's law can be stated as:

$$\left[\frac{dP}{dx}\right]_f = K_1\left(\frac{\mu_L}{\rho_L}\right)\left(\frac{W_L}{A_t}\right) \qquad \text{... D-13}$$

where K_1 is a proportionality constant, and A_t is the total cross-sectional area of wick normal to liquid flow.

However,

$$F_f = \frac{dP}{dx}\Big|_f dx\ \varepsilon\delta b \qquad \text{... D-14}$$

where F_f is the frictional force of liquid flow.

Hence

$$F_f = K_1\varepsilon^2\,\delta b\,\mu_L u_L dx \qquad \text{... D-15}$$

Thus the momentum equation in the x-direction reduces to:

$$-2\sigma\frac{dR}{R^2} - \varepsilon K_1\mu_L u_L dx = \frac{\rho_L}{g_o}\frac{d(u_L)^2}{dx}\cdot dx \qquad \text{... D-16}$$

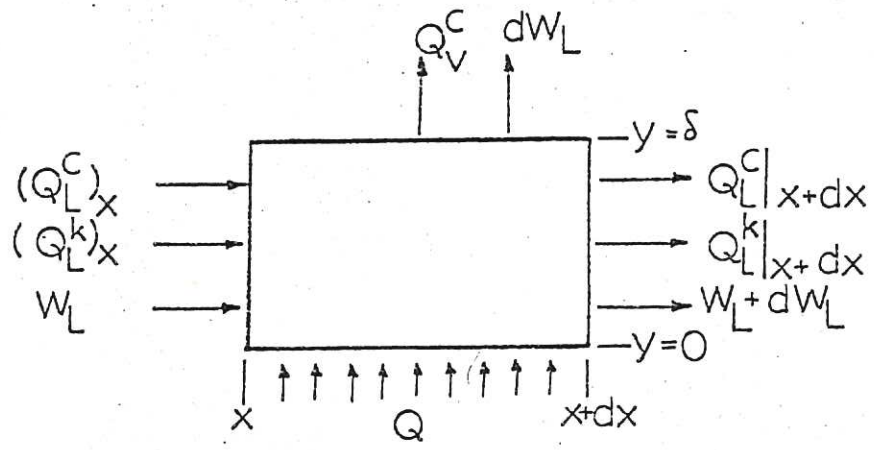

FIGURE H-2. An Energy Balance for a Differential Element of Wick

An energy balance for a differential element of wick yields;

$$(Q_L^c)_x - Q_v^c + Q = (Q_L^c)_{x+dx}, \qquad \text{... D-17}$$

where Q_L^c is the heat transferred by convection of the liquid and Q is the applied heat input per unit time. The energy leaving at the top surface of the element is;

$$Q_v^c = W_v h_v \qquad \text{... D-18}$$

$$= -h_v \rho_L \left(\frac{du_L}{dx}\right) dx \varepsilon \delta b \qquad \text{... D-19}$$

where h_v is the specific vapour enthalpy.

Hence,

$$-u_L \rho_L \frac{dh_L}{dx} + (h_v - h_L)\rho_L \frac{du_L}{dx} + \frac{q}{\delta\varepsilon} = 0 \qquad \text{... D-20}$$

but

$$\frac{du_L}{dx} = -\frac{q}{h_{LV} \delta \varepsilon \rho_L} \qquad \text{... D-21}$$

hence integrating this equation;

$$u_L = \frac{q}{h_{LV} \delta \varepsilon \rho_L}(1-x); \qquad \text{since } u_L = 0 \text{ when } x = 1 \qquad \text{... D-22}$$

and

$$W_L = \frac{qb(1-x)}{h_{VL}} \qquad \text{... D-23}$$

The energy and momentum equations may be combined to give:

$$\sigma \left(\frac{\rho}{\sigma}\right)_{WR} l_m = \frac{q\mu_L l^2}{2h_{LV} \delta \rho_L g_o} K_1 \qquad \text{... D-24}$$

where $(\rho/\sigma)_{WR}$ is the density/surface tension ratio appertaining to wick rise tests. If gravity forces are taken into account and the wick is inclined at angle θ to the horizontal, then:

$$\sigma \left(\frac{\rho}{\sigma}\right)_{WR} l_m = \frac{q\mu_L l^2 K_1}{2h_{VL} \delta \rho_L g_o} - \rho_L \sin\theta . l. \qquad \text{... D-25}$$

This equation gives the maximum heat flux as limited by the capillary pumping power of the wick. The fluid properties enter as the dimensional parameter;

$$N = \frac{\rho_L h_{VL} \sigma}{\mu_L} \qquad \ldots D\text{-}26$$

To maximise the performance of the evaporator a liquid should have as large a value of N as possible. Values of N are given below;

Liquid	N (Btu.hr.lbf/ft^3.lbm)		
	at 70°F	at 1300°F	at boiling point
sodium	-	1983	2016
potassium	-	406	411
water	138	-	336
freon 12	5.2	-	-

Table D-1

The only quantity in equation H-25 which is not directly measurable is l_m, the maximum rise of liquid in a vertical wick when exposed to a gravity field. The usual method of determining the effective minimum radius of curvature in a wicking material is to observe the maximum height to which the liquid rises in a vertical sample of the wicking material. If the pores in the vertical wick through which the liquid rises can be thought of as single capillary tubes of an equivalent diameter, the effective minimum radius of curvature is;

$$R_{min} = \frac{2g_o \sigma}{\rho_L g l_m} \qquad \ldots D\text{-}27$$

where l_m is the maximum height of the liquid in the vertical wick when exposed to a gravity field g. The evaporator heat flux is maximised when l_m/K_1 is large. The constant K_1 is a measure of the magnitude of the frictional forces associated with a flow of liquid through the wick under conditions where Darcy's law applies. This constant is obtained by measuring the pressure drop across a wicking sample through which a given amount of liquid is flowing.

The effect of the capillary pumping power of a wick sample on the operation of an overlaid evaporator may thus be determined by measurement of the quantity l_m/K_1.

Three types of porous wicks are suitable for use in a potassium cooled blanket for a fusion reactor due to their ease of fabrication, dimensional stability,

isotropy and thermal conductivity. These are:

Type	Typical porosity range	Permeability range ($1/ft^2$)
sintered screen materials	$60\% < \varepsilon \leq 70\%$	$1 < K_1.10^{-8} \leq 12$
sintered powder materials	$45\% < \varepsilon \leq 70\%$	$3 < K_1.10^{-8} \leq 11$
sintered fibre materials	$60\% < \varepsilon \leq 95\%$	$0.8 < K_1.10^{-8} \leq 62$

Table D-2

Typical median pore diameters of such wicks have been measured by Kunz et al[23] and vary from 20 to over 100 microns. Equilibrium height to which water will rise in vertical samples of the wick vary from two to over 16 inches. In general, sintered screens tend to produce the lowest vertical rises and sintered fibres the highest.

Sintered fibres exhibit the best (l_m/K_1) ratios and are recommended for potassium fusion blanket cooling application. In general, (l_m/K_1) is found to increase with pore size for a range of pore sizes from 0-250 microns. This is due to the fact that the capillary forces are inversely proportional to the effective pore diameter whereas the frictional forces are inversely proportional to the diameter squared.

The maximum capillary pumping capacity of a wick is thus dependent on the value of the group (l_m/K_1) when zero net body forces are considered. Sintered fibre wicks are preferred have (l_m/K_1) values as high as $5.10^{-9}(ft^3)$. In applications involving a condition in which a capillary pump works against gravity consideration must be given both to the capillary pumping parameter (l_m/K_1) and to l_m, the equilibrium height of liquid in the vertical wick.

Limitation due to Wick Boiling

The process occurring in an overlayed wick evaporator can be visualised in the following manner. As heat is initially added in the evaporating region, the heat will be conducted through the solid wall and the wick-liquid composite to the vapour-liquid interface where evaporation takes place. As the heat input is increased the liquid wick-solid interface temperature will rise to the point where

the adjacent liquid is sufficiently superheated to cause nucleate boiling at the interface. If an equilibrium condition is to occur without excessive superheat, the capillary and buoyancy forces must be great enough to cause convection of the resulting vapour through the wick to the vapour cavity and supply fresh liquid to the heating surface at sufficient rate. If the vapour does not leave the interface at the rate at which it is produced, liquid is excluded from the surface, film-boiling sets in and the heat transfer characteristics of the surface fall sharply.

In Appendix C a theoretical model of boiling in a porous wick is given. A description is given here of experimental studies of boiling in wicks.

Tests have been performed by Kunz et al[28] to determine the variation of heat flux with ΔT_{SAT} (the temperature difference between the liquid-wick and the saturation temperature) and also the maximum heat flux that can be sustained before film boiling occurs. Heat fluxes up to 0.28 MW/m^2 were reported with sintered nickel screen type wicks, heat fluxes up to 0.568 MW/m^2 with sintered nickel powder wicks and fluxes of up to 0.570 MW/m^2 with sintered nickel fibre wicks using water as the heat transfer fluid. Grooving of the wick improves the maximum heat flux by up to 40%.

To determine the effect of fluid properties or boiling from wick covered surfaces Kunz et al[29] repeated boiling tests with water and Freon 113 and the following relationship was found to hold within experimental accuracy.

$$\frac{(q)^{\text{critical}}_{\text{fluid}}}{(q)^{\text{critical}}_{\text{water}}} = \frac{\lambda_{\text{fluid}}}{\lambda_{\text{water}}} \left(\frac{\rho_{L\ \text{fluid}}}{\rho_{L\ \text{water}}}\right)^{0.6} \left(\frac{\rho_{v\ \text{fluid}}}{\rho_{v\ \text{water}}}\right)^{0.4} \qquad \ldots \text{D-28}$$

This equation may be used to estimate the maximum heat flux permissible in a potassium or a sodium filled metal fibre wick. This is given below:

Fluid	(q_{crit}) fluid/(q_{crit}) water	(q_{crit}) fluid
potassium	0.633	0.360 MW/m^2
sodium	1.149	0.655 MW/m^2

The limiting heat fluxes for the above cases may be evaluated if it is assumed that capillary pumping capacity is the limiting factor. From the previous section:

$$\sigma\left(\frac{\rho}{\sigma}\right)_{WR} l_m = \frac{q_E \mu_L l_E^2 K_1}{2h_{VL}\delta\rho_L g_o} - \rho_L \sin\theta\, l_E \qquad \ldots \text{D-29}$$

and this equation may be used to estimate the capillary pumping limited heat flux. For a sintered stainless steel fibre wick, this yields (q_{crit}) for potassium of 2.9 MW/m^2 and (q_{crit}) sodium of 5.3 MW/m^2. It appears therefore that vapour blanketing is the more serious limitation for overlayed wick evaporating surfaces in a potassium cooled fusion blanket.

Summary

In this appendix, experimental data for heat transfer to laminar flow in wick systems has been examined. The effects of superimposed magnetic fields have not been considered. The analysis of appendix C indicates however that magnetic fields may appreciably reduce maximum possible heat transfer rate in potassium filled wicks. In this appendix, experimental data relevant to the asymptotic case of zero magnetic field intensity is presented. It is found that;

1) A simplified analysis indicates that the maximum height to which a liquid will rise in a vertical wick, l_m, and the friction factor K_1 are the important parameters in determining the capability of a capillary pump in an overlayed wick evaporator.

The theory indicates that the larger the value of the capillary pumping parameter $\left(\frac{l_m}{K_1}\right)$ the better the capillary pump when head effects due to gravity are negligible.

2) Sintered fibre wicks produced the best capillary pumping characteristics followed by the sintered powder wicks. The sintered screen samples demonstrated lowest potential as capillary pumps.

3) Limiting heat transfer rates for boiling are highest for the sintered fibre examples. Values of over 0.5 MW/m^2 have been experimentally measured using water as the test fluid. This corresponds to heat fluxes of 0.36 MW/m^2 for potassium and 0.65 MW/m^2 for sodium.

4) Limitations on evaporator output caused by vapour blanketing appear to be more severe than limitations imposed by constraints of capillary pumping power.

The presence of a magnetic field will suppress boiling and give rise to greater superheat, but it has been suggested that boiling can be initiated by "artificial cavities". In fact, in one study, a metal ring close fitting on a tube has been used to do this - the cavities being formed between the inside of the ring and the outside of the tube. It is quite likely that in a sintered fibre wick, similar artificial cavities will be formed where the fibres cross.

APPENDIX E

Circumferential Variation of Magnetic Field

In computing the overall pumping power requirements for providing the coolant supply to the blanket it is necessary to make allowance for the variation of magnetic field with minor toroidal angle.

Referring to figure A-1 the variation of magnetic field within the space BC is:

$$B_{(\phi)} = B_{max} \left\{ \frac{R_B}{R_B + r_{mi}\,(1 - \cos\phi)} \right\} \qquad \text{E-1}$$

where ϕ is the minor toroidal angle, as shown in figure E-1

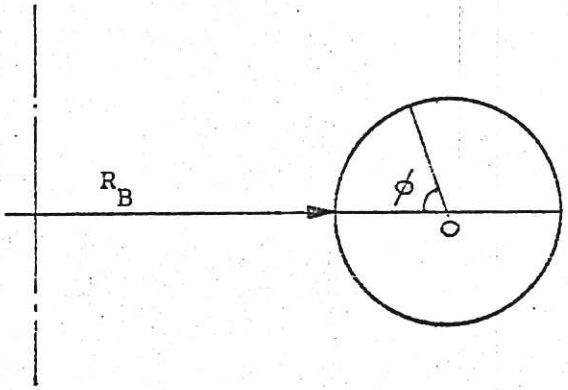

Figure E-1

For various wall loadings it is possible using equation E-1 to relate the average MHD pressure drop in supplying coolant to the blanket cells to the maximum MHD pressure drop. In table E-1 this information is presented for reactor wall loadings of 1,5 and 10 MW/m^2 and is necessary for computing pumping power requirements.

Reactor Wall loading (MW/m^2)	1	5	10
Ratio of mean MHD pressure loss in primary circuit to maximum MHD pressure loss	0.605	0.528	0.477

Table E-1

Whereas the stressing of the blanket is evaluated at the most critical part of the blanket (where the primary coolant circuit pressure drop is highest) the pumping power requirements are evaluated on the basis of the mean primary circuit pressure loss.

Appendix F

Optimization of Duct sizes

Because the greater part of the pressure loss in the primary coolant circuit occurs in the cell liquid inlet manifold and inlet ducts, circuit pressure drop can be minimized by the correct apportioning of areas to inlet and outlet ducts. Computations of the relative sizes of inlet and outlet ducts have been made by assuming that the total area of the ducting is one tenth the area of the inner magnet surface. The restriction is made that the Mach number of vapour in the outlet duct shall not exceed 0.3 and compressibility effects are included in the analysis.

With these assumptions the following table of optimal duct sizes is found.

wall loading (MW/m^2)	max. magnetic field (tesla)	potassium inlet duct dia. (m)	potassium outlet duct dia. (m)
1	7	0.21	0.07
5	14	0.23	0.096
10	19	0.24	0.12

Table F-1

Optimal coolant inlet and outlet duct dimensions per blanket cell.

APPENDIX G

Heat Transfer and Pressure Drop Calculations for the Field-Aligned Boiling Configuration

In order to compute the required area of cooling surface it is necessary to evaluate the maximum (or critical) heat flux from the lithium to the potassium coolant. If the liquid potassium flow is assumed to be laminar a lower bound on the critical heat flux is given by:

$$(\phi \text{ crit})_{min} \geq \frac{(\Delta T \text{ sub})_i}{\left\{ {}^{4z}/_{Gc_{pL}D} + {}^{1}/_{h_{fo}} \right\}} \quad \ldots\ldots \text{G-1}$$

assuming (1) a wall loading of $4 MW/m^2$

(2) h_{fo} for a typical geometry is $2200 W/m^2 {}^{\circ}C$

(3) $(\Delta T \text{ sub})_i$ the inlet subcooling $\approx 200^{\circ}C$

then a lower bound on the critical heat flux from equation G-1 is $0.23 MW/m^2$.

An upper bound for the critical heat flux is given by equation G-2.

$$(\phi \text{ crit})_{max} \leq \frac{GD\lambda}{4z} \left\{ 1 + \frac{c_{pL} (\Delta T \text{ sub})_i}{\lambda} \right\} \quad \ldots\ldots \text{G-2}$$

If the above assumptions are used then $(\phi \text{ crit})_{max}$ is $5.88 MW/m^2$. The critical heat flux thus lies in the range $0.23 MW/m^2$ to $5.88 MW/m^2$.

A more accurate estimation of the critical heat flux may be gained from the Noyes and Lurie (1966) correlation for pool boiling of sodium:

$$q_{crit} = (4.0 + 1.75\, p^{0.457}) \times 10^5 \times 3.155 \; W/m^2 + q_{conv} \quad \ldots \text{G-3}$$

where p is the applied pressure (in psia),

and q_{conv} is the convective contribution to the critical heat flux

hence $q_{crit} = 3.155 \times 10^6 + \frac{Nu\, k_L}{D} (\Delta T) \quad \ldots\ldots \text{G-4}$

where q_{conv} is estimated (conservatively) by ignoring enhancement due bubble agitation. A temperature difference of $55^{\circ}C$ is assumed between the duct and the bulk liquid, estimated in accordance with the data of Madsen and Bonilla (1961).

Equation G-3 yeilds a critical heat flux of $3.3 MW/m^2$. Fraas[8] has observed that intense magnetic fields apparently have little effect on the critical heat flux. Most boilers are operated at heat fluxes 1/10 to $\frac{1}{4}$ of the critical heat flux and thus a heat flux of nearly $1 MW/m^2$ could be sustained in the coolant tubes of a blanket cell. This is an order of magnitude greater than that given by helium cooling.

Heat Transfer to the Potassium Feed

For fully developed laminar flow through a pipe:

$$Nu = \frac{hd}{k} = 4.12 \qquad \text{G-5}$$

so that the convective heat transfer coefficient at feeder pipe inner wall

$$h_f = 4.12\ k_L/d_f = 2200\ W/m^2\,^\circ C \qquad \text{G-6}$$

For conduction through the feeder pipe wall

$$\text{then } h_w = \frac{K_{dw}}{t_{dw}} = 11{,}350\ W/m^2\,^\circ C \qquad \text{G-7}$$

where K_{dw} is the thermal conductivity of the duct wall

L_{dw} is the thickness of the duct wall

the heat transfer coefficient at the outside of the feeder pipe is assumed infinite. This is strictly not true and will result in a slight overestimation of the heat flux to the feeder pipe.

combining the above coefficients gives a total coefficient of

$$h_f = 1840\ W/m^2\,^\circ C$$

To evaluate the heat generated within the feeder pipe and potassium feed it is assumed that potassium and structure internal heat generation rates are equal. From figure 9, heat production in the feeder pipe is $0.0063P_w$. Hence heat transferred to potassium in the feeder pipe is

$$\left\{ h\,\pi\,d_f\,l_f\,\Delta T_{fc} + 0.0063P_w \right\} \quad \text{where } P_w \text{ is measured in } MW/m^2.$$

At all wall loadings the feeder temperature rise can be maintained below 300°C. In order to avoid two phase flow in the inlet manifold of each blanket cell a subcooling of at least 300°C is thus required at exit from the primary circuit heat exchanger.

Heat Transfer in the Cell Outlet Manifold

From Owen, Hunt and Collier[7] it is advantageous to avoid two phase flow in the outlet manifold in order to minimise MHD pressure drop in the primary coolant circuit. If a dryout condition is assumed at the outlet end of the field-aligned boiling region then the heat transfer coefficient in the cell outlet manifold may be estimated from the McAdam's correlation to be approximately 100 $W/m^2\,^\circ C$. If a large number of liquid droplets are present in the potassium vapour, the heat transfer coefficient may be estimated by assuming a film boiling mechanism. From Padilla and Balzhiser (1967) heat transfer coefficients

of the order 200-300 $W/m^2{}^oC$ may be estimated. These estimates of heat transfer coefficients in the outlet manifold region indicate that there is poor transfer of heat from the lithium to the potassium in this region. This implies that either:

(1) lithium temperatures in this region will be higher than elsewhere in the cell so that heat may be conducted to the cooling tubes wetted with liquid potassium, or

(2) some 2-phase flow of potassium has to be accepted in the outlet manifold of each cell.

Pressure Drop in the Field-Aligned Region

When no twisted tapes or similar devices are used, the two phase pressure drop in the field-aligned boiling region is computed by assuming a linear change of quality. The liquid phase is assumed to be laminar and the pressure drop is entirely frictional. Hence:

$$\Delta P_{TP} = \frac{2 f_{TP} L G^2 U_f}{D} \left\{ 1 + \frac{x}{2} \frac{V_{fg}}{V_f} \right\} + G^2 v_f \left\{ \frac{V_{fg}}{V_f} \right\} x \quad \ldots \text{G-8}$$

where ΔP_{TP} is the two-phase pressure drop

f_{TP} is a two-phase friction factor (assumed to be 0.05)

G is a mass velocity

X is the quality at the end of the field-aligned region

L is the length of the region

V_f is the specific volume of the liquid phase

V_{fg} is the difference in specific volumes between the gaseous and liquid phases.

For 20 cooling tubes of 2 cm diameter the two phase pressure drop is 1.26×10^3 N/m^2 at a wall loading of 1 MW/m^2, 3.1×10^4 N/m^2 at a wall loading of 5 MW/m^2 and 1.26×10^5 N/m^2 at a wall loading of 10 MW/m^2.

When twisted tapes are used to prevent the early onset of dryout, the dominant pressure drop is caused by the induced swirl which necessitates motion of the liquid potassium transverse to the magnetic field. This MHD pressure drop is estimated as follows:

(1) Assume the helical insert has a pitch to diameter ratio of 3. This figure is typical of inserts used by NASA[15] for space powerplant application.

(2) Assume a linear variation of quality along the cooling duct.

(3) Assume the liquid remaining at any section traverses a path at an effective diameter equal to the tube radius

(4) Assume the number of cooling tubes is adjusted to give a heat flux of 0.5 MW/m^2 over the surface of the cooling tubes.

The average liquid velocity for the two phase region is then computed and the MHD pressure drop obtained from:

$$MHD = U_s (\sigma_e \phi)_D \cdot L_p \quad B_{max}^2 \qquad G\text{-}9$$

where U_s the mean swirl velocity in the 2 phase region , $(\sigma_e \phi)_D$ is the product of the potassium electrical conductivity and the wall conductance ratio for the cooling tube and L_p is the effective path length of the swirling flow transverse to the magnetic field.

At a wall loading of 1 MW/m^2 the two-phase pressure drop is 4.2×10^5 N/m^2. When the wall loading is increased to 5 MW/m^2 the pressure drop becomes 1.68×10^6 N/m^2 and at a wall loading of 10 MW/m^2 the two-phase pressure drop is 3.1×10^6 N/m^2. The use of twisted tapes to prevent slow quality dryout thus incurs a heavy pressure drop penalty.

APPENDIX H

Structure Fraction and Pumping Power Considerations:

Structure fraction for wicked cell:

The following assumptions have been made in computing the structure fraction:

(1) Cell Walls, and wicked surfaces are 0.2 cm thick

(2) First wall is 1.5 cm thick

(3) Porous overlaying is not included in the estimates of structure fraction which are consequently slightly optimistic

Total volume per blanket cell is 0.3 m^3. Volume of casing assuming a right parallelepiped geometry is 0.0109 m^3. Structure volume of overlayed plates is 0.0006N m^3 where N is the number of plates. Table H-1 gives the structure fraction as a function of the number of overlayed plates:

Number of Overlayed Plates	Structure Fraction
1	0.038
5	0.046
10	0.056
15	0.066
20	0.076

Table H-1 Structure fraction for the Wicked Configuration

Structure Fraction for the once through evaporator

Cooling tubes are assumed to be 1.25 cm diameter and of thickness 0.2 cm. Casing volume is identical to that of the wicked configuration and structure volume of cooling tubes is 0.0001 M. m^3 where M is the number of cooling tubes. Table H-2 gives the structure fraction as a function of the number of cooling tubes.

Number of Cooling Tubes	Structure Fraction
20	0.043
40	0.049
60	0.056
80	0.063
100	0.069

Table H-2 Structure fraction for the once-through evaporator

Pumping Power Requirements

Power required for circulating coolant per cell is the product of the volume flowrate per cell and overall pressure drop in the primary circuit. Total input power per cell is 0.3 of the wall loading. Hence the ratio of pumping power to reactor power varies with wall loading. At a wall loading of 1 MW/m^2, pumping power is only 0.0030% of reactor output. At a wall loading of 5 MW/m^2 the pumping power has increased to 0.042% of the reactor output. At a wall loading of 10 MW/m^2 the pumping power requirement is 0.2% of the reactor output. Allowance has been made for the variation of pressure losses with minor toroidal angle in computing these figures (refer Appendix E).

APPENDIX I

Sodium as a Topping Fluid for a Steam Rankine Cycle

This Appendix examines the feasibility of employing a sodium vapour topping cycle in conjunction with a steam Rankine cycle.

The number of stages required in a sodium turbine may be estimated from Horn and Norris* as 18 whereas 6 to 8 are required for potassium. The exhaust area per unit output from the sodium turbines (which governs the turbine size and ~~cost~~ cost) is proportional to $1/MP_cL_c^{1.5}$ where M is the latent heat of the sodium at the condenser pressure. Values of $MP_cL_c^{1.5}$ are given in table I-1 below for sodium and are compared with corresponding values for steam and potassium.

Fluid	Turbine Exhaust Temperature	$MP_cL_c^{1.5}$
Steam	25°C	3.117×10^5
Steam	30°C	3.654×10^5
Steam	35°C	4.244×10^5
Potassium	500°C	5.780×10^5
Potassium	550°C	1.347×10^6
Potassium	600°C	2.551×10^6
Sodium	600°C	8.1×10^5
Sodium	650°C	1.72×10^6
Sodium	700°C	3.34×10^6

Table I-1 Inverse Turbine Exhaust Area Parameter

The reduction in size of a liquid metal turbine over a corresponding steam turbine operating at 30°C exhaust temperature is given below in Table I-2.

Fluid	Exhaust Temperature	Reduction in Size over a steamturbine
Potassium	500°C	0.633
Potassium	550°C	0.27
Potassium	600°C	0.14
Sodium	600°C	0.384
Sodium	650°C	0.212
Sodium	700°C	0.127

Table I-2

*Horn G, Norris T.D. and Whybrow J.F.T. "Turbine flow problems of binary cycles ... high density fluids" I.M.E. Volume 183 Part I No. 8 (1968)

The comparative temperatures in the sodium and water circuits are of importance. In particular, consideration must be given to matching the temperatures across the linking heat exchanger. In order that excessive heat fluxes are avoided it is desirable to maintain a temperature difference across the heat exchanger tubes of 11°C- 27°C+. The sodium turbine exit temperature can be matched with the steam turbine inlet temperature by adopting a recycle method+ without sacrificing efficiency.

The overall sodium/steam cycle efficiency may be computed as a function of changeover temperature. In Table I-3 the relevant efficiencies are given:

Sodium condenser/ steam top temperature	600°C	700°C	800°C	900°C
Sodium cycle efficiency	0.376	0.272	0.168	0.0644
Overall efficiency	0.647	0.588	0.53	0.47

Table I-3 Sodium-steam cycle efficiencies

Thus sodium may be used in a topping cycle for a steam Rankine cycle provided suitable steps are taken to properly link the cycles. Overall efficiencies are similar to those achievable with a potassium topped steam cycle.

+"Potassium ~~cond~~ topped steam cycle for power generation" N Hall - Taylor, Rolls-Royce Future Project Study (FPS.208)

Appendix J. The 100-group nuclear data library

The basic source of all the nuclear data was the ENDF/B-III library, but to reduce the data handling problem to acceptable proportions the cross-sections required for neutron transport were abstracted from the DLC-2 library[30]. The latter is a standard 100-group library reduced from ENDF/B-III data using the SUPERTOG-III code[31], and was generated using a flux weighting spectrum formed by joining a fission spectrum to a $^1/E$ tail at 0.0674 MeV. While this spectrum is obviously not appropriate to fusion blanket calculations, it introduces a comparatively small error when used to produce a 100-group library though for further group collapsing an appropriate spectrum calculation would be necessary. To avoid this complexity, all the calculations were performed using 100 groups. One dimensional cross-section sets required for reaction rate analysis were processed at Harwell using SUPERTOG-III and ENDF/B-III, and, for consistency, using the same weighting spectrum. The one exception was the ^{7}Li (n, n'α)t set which was abstracted from UKNDL[32].

Appendix K. The Accuracy of the Neutron Transport Calculations

The computational overheads and the complexity of nuclear data handling are strongly influenced by the order of angular quadrature and the number of terms used in the expansion of the scattering cross-sections. A brief study was, therefore, undertaken to match the accuracy achieved in the use of the ANISN programme to the accuracy justified by the nature of the problem.

The case chosen for investigation was the wicked cell with 5 $MW.m^{-2}$ wall loading with TZM as the structural material. A series of calculations was performed in which the order of quadrature was increased from S_4 to S_{12} and the order of scattering from P_o to P_3. Higher orders were felt to be inappropriate to survey calculations, and this was confirmed by the results produced. The integral results for tritium breeding are listed in table 7. It should be noted that, as expected, the predicted breeding ratios decrease as the orders of approximation increase, so that very low order calculations are undesirably optimistic. The $^6Li\ (n,\alpha)\ t$ reaction is seen to be more affected than the $^7Li\ (n, n'\alpha)t$ reaction, which results from its greater dependence on an adequate representation of slowing down and thermalization. In figures 12 and 13 the distribution of these reactions across the length of the cell is plotted for three of the approximations, and both show that the $S_4 - P_o$ calculation is inadequate to describe the transport characteristics across the cell, whereas the $S_8 - P_1$ and $S_{12} - P_3$ results differ only marginally. The greatest difference between these two latter approximations is for ^7Li near the outer boundary of the cell, but this region produces an insignificant contribution to the total ^7Li reaction rate.

The scale of approximations introduced by the present simplified model of a toroidal reactor leads to an overestimate of up to 10% in tritium breeding predictions and the uncertainties in the nuclear data to an error which is probably in excess of $\pm 5\%$ (20). A neutron transport calculation which contributes a further $\pm 1\%$ error is quite adequate. The difference in total tritium breeding ratio between the $S_8 - P_1$ and $S_{12} - P_3$ calculations is 0.34%, and the difference between the $S_{12} - P_3$ result and the asymptotic value is unlikely to exceed 0.5%. Thus the total systematic error

in the $S_8 - P_1$ case is less than 1%. This approximation was therefore used for all further calculations.

Appendix L The effect of a change in the reactor model

It has been assumed in the main text of this report that the reactor model has the following parameters: (Culham conceptual design MkI)

Power output 2500 MW(e), aspect ratio of plasma = 6

aspect ratio of first wall = 4.8, $\eta = 0.32$

Some recent conceptual reactor designs have tended towards a reactor model having the following parameters listed below: (Culham conceptual design MkII)

Power output 2500 MW(e), aspect ratio of plasma = 3;

aspect ratio of wall = 2.4; $\eta = 0.32$

(More detailed information on this design is given in table L-1)

The second conceptual design given above will yield a different plasma equilibrium requirement to the original design. The two curves for plasma equilibrium are shown in figure L-1 for comparison. When the stress limitation curves of figure 6 or 11 are superimposed on the plasma equilibrium requirement curves it may be observed that the maximum wall loading (for a given maximum stress in the coolant ducting) is little different for the new design than for the original design. Changing the aspect ratio of the plasma from 6 to 3, therefore, has little effect on the maximum wall loading of the reactor.

The maximum wall loading of the MkI design is, thus, or sodium. also expected to lie within the range 5-7 MW/m² if potassium is used as the blanket coolant.

Table L - 1

Main machine parameters for Culham MkII conceptual design

$\eta = 0.32$; $A_{plasma} = 3$, $A_{wall} = 2.4$

Wall loading (P_w)	1.1	3.3	11	(MW/m^2)
energy/unit area wall (P)	1.0	3.0	10	(MW/m^2)
major radius of torus (R_M)	20.84	11.47	6.59	(m)
minor radius of torus (r_m)	8.68	4.78	2.75	(m)
inner magnet radius (R_{mi})	10.48	6.58	4.55	(m)
maximum magnet field	5.24	9.55	19.9	(Tesla)

blanket thickness = 1.8 metres

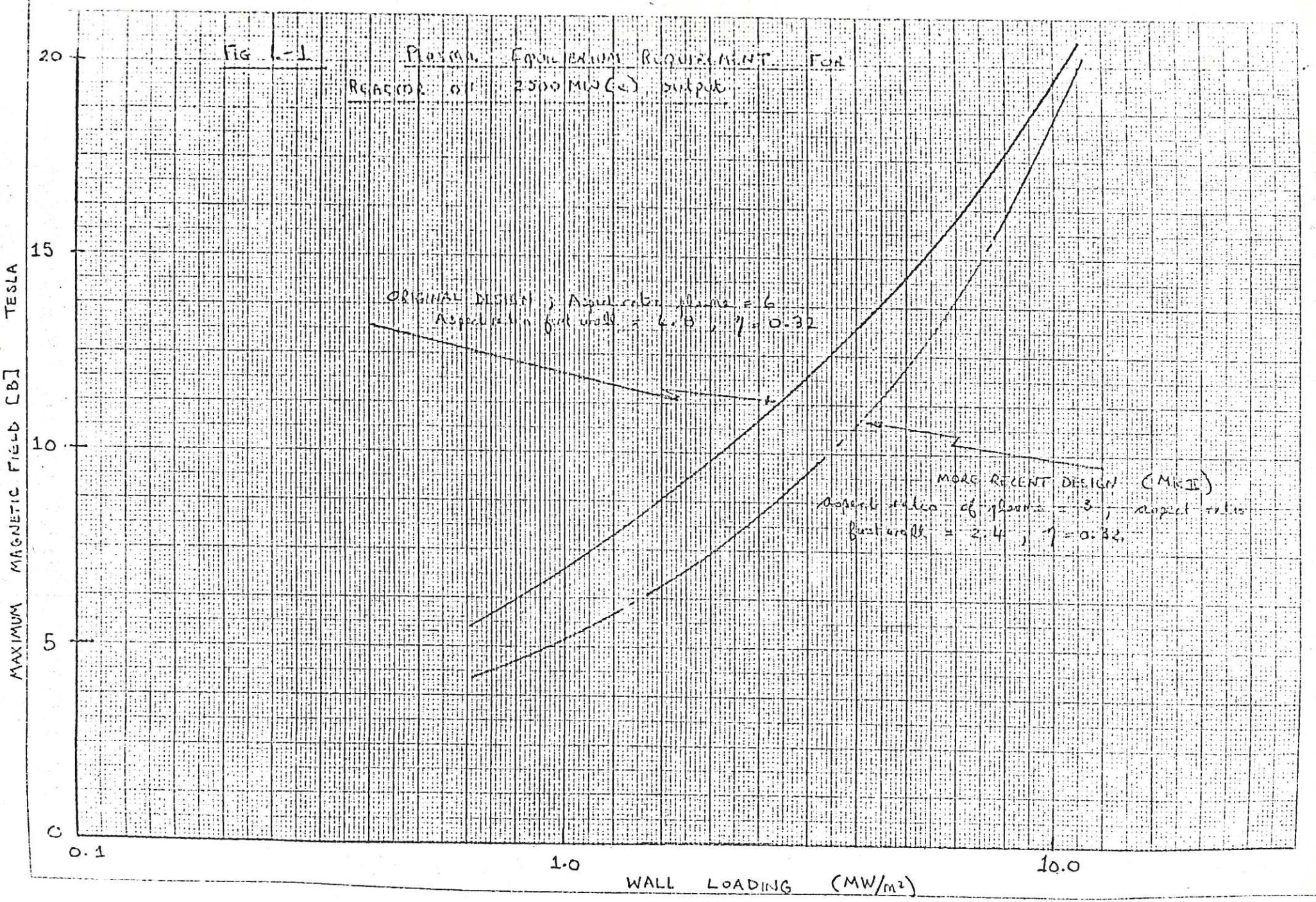
Fig 1.-1 Plasma Equilibrium Requirement for Reactor of 2500 MW(e) output
ORIGINAL DESIGN ; Aspect ratio plasma = 6
Aspect ratio of coil = 4.8 , η = 0.32
MORE RECENT DESIGN (MK II)
Aspect ratio of plasma = 3 , aspect ratio
coil = 2.4 , η = 0.32
MAXIMUM MAGNETIC FIELD [B] TESLA
20
15
10
5
0
0.1
1.0
10.0
WALL LOADING (MW/m²)